A THEORETICAL MODEL FOR ESTIMATING DIFFUSION WEAR IN METAL CUTTING

by

SURJYA K. PAL

DEPARTMENT OF MECHANICAL ENGINEERING

INDIAN INSTITUTE OF TECHNOLOGY KANPUR

JUNE, 1993

A THEORETICAL MODEL FOR ESTIMATING DIFFUSION WEAR IN METAL CUTTING

A Thesis Submitted

in Partial Fulfilment of the Requirements

for the Degree of

MASTER OF TECHNOLOGY

by

SURJYA K. PAL

to the

DEPARTMENT OF MECHANICAL ENGINEERING

INDIAN INSTITUTE OF TECHNOLOGY, KANPUR

JUNE, 1993

CERTIFICATE

7.6.93

This is to certify that the thesis entitled "*A THEORETICAL MODEL FOR ESTIMATING DIFFUSION WEAR IN METAL CUTTING*" which is being submitted by *Surjya K. Pal* to the Mechanical Engineering Department of Indian Institute of Technology, Kanpur, in partial fulfilment for the award of Master of Technology, is a record of bonafide work carried by him under our supervision and guidance.

T. Sundararajan
Dr. T. Sundararajan

Dr. G. K. Lāl

Department of Mechanical Engineering

Indian Institute of Technology

Kanpur

Date: 3.6.1993

TO

MY BELOVED PARENTS

ACKNOWLEDGEMENT

I would like to express my deep sense of gratitude to Dr. T. Sundararajan for his valuable suggestions, constant encouragement, meticulous attention and above all, endless sharing of time with me till late in the night —— has given me a new dimension. Discussions with him for several hours created an unlimited thirst for knowledge inside me. I am extremely charmed by his pleasing personality and cool behaviour.

I am thankful to Dr. G. K. Lal for his suggestions for the formulation of the thesis work.

I feel very fortunate to have the oppurtunity of getting them as supervisors.

I am grateful to Dr. G. Biswas for his showering of blessings on me and also for mental consolation during the critical time of my thesis work.

My IIT Kanpur life has been spiced by my friends. Anir, Parthas, Partha, Smitra, Msarkar, Abray, Sirde —— they are in my heart and will be. Helping hand from Joydip, Parit, Bpm, Sneh, Manab, Nvr, in so many occasions, is really unforgettable —— I am proud of having such a lot of good friends at IIT Kanpur.

I also express my sincere gratitude to my family members for showing considerable patience during my long absence from home. My achievement is much much less than their sacrifice. Without their cooperation, the present work would have been an impossibility.

June, 1993

SURJYA K. PAL

CONTENTS

LIST OF FIGURES

LIST OF TABLES

ABSTRACT

A theoretical model for the prediction of the temperature field and the concentration field of diffusing species in the vicinity of the cutting edge during orthogonal machining has been developed. The finite element method has been applied to solve the steady heat transfer and transient species transport equations in two dimensions. The changes in the thermal properties and diffusion coefficient with temperature have been accounted for. Based on the temperature and concentration solutions, changes in the strength of the tool material with time at each location have been predicted, assuming carbon diffusion. Comparing the local strength with the actual stress, regions which are likely to undergo wear have been identified. A few typical machining situations have been analysed and results show reasonable agreement where comparisons are possible. The present approach has promise for being a valuable theoretical aid for analyzing tool wear due to diffusion at high cutting speeds.

NOMENCLATURE

SYMBOLS	DESCRIPTION (UNITS)
c	Carbon concentration (%)
c_p	Specific heat (J/kg K)
D	Diffusion coefficient (m^2/s)
D_0	Pre-exponentional constant (m^2/s)
D_1	Diameter of the workpiece (mm)
delta2	Thickness of the secondary zone (mm)
f2a	Shear stress in sticking portion (N/mm^2)
f2b	Shear stress in sliding portion (N/mm^2)
fh	Horizontal component of cutting force (N)
fn	Normal to frictional force (N)
fs	Shear force (N)
fsn	Normal to shear force (N)
fv	Vertical component of cutting force (N)
h'	Overall heat transfer coefficient (w/m^2K)
h_x	Length of the tool (mm)
h_y	Height of the tool (mm)
h	Total contact length (mm)
k	Thermal conductivity (w/mk)
l_{sl}	Sliding contact length (mm)

l_{st}	Sticking contact length (mm)
N	Rpm of the workpiece
PSDZ	Primary shear deformation zone
$\dot{Q}$	Volumetric heat generation rate (w/m^3)
$\dot{Q}_{pz}$	Heat generation rate per unit volume in primary zone (w/m^3)
$\dot{Q}_{2a}$	Heat generation rate per unit volume due to plastic work in secondary zone (w/m^3)
$\dot{Q}_{2b}$	Heat generation rate per unit volume due to frictional work in secondary zone (w/m^3)
q	Activation energy for diffusion (KJ/mol)
R	Gas constant (J/molK)
r	Chip thickness ratio
SSDZ	Secondary shear deformation zone
T	Absolute temperature (K)
T_{amb}	Ambient temperature (K)
t	Depth of cut (mm)
t_c	Chip thickness (mm)
u	Cutting velocity in X - direction (m/s)
v	Cutting velocity in Y - direction (m/s)
vs	Shear velocity (m/s)
V	Cutting velocity (m/s)
V_{chip}	Chip velocity (m/s)
V_{int}	Interfacial velocity (m/s)
w	Width of cut (mm)

x	Coordinate in cutting direction
y	Coordinate normal to the cutting direction
yst	Yield stress in the tool material

GREEK SYMBOLS

α	Rake angle (degrees)
δ	Clearance angle (degrees)
η	Local y - coordinate
ϕ	Shear angle (degrees)
ρ	Density (kg/m^3)
σ	Stress (N/mm^2)
ζ	Local x - coordinate

SUBCRIPTS

amb	Ambient
chip	Chip of the Workpiece
int	Interfacial
i	Used to denote different regions
TS	Tensile
YS	Yield

CHAPTER 1

INTRODUCTION

1.1 GENERAL BACKGROUND

The importance of machining in the modern engineering industry need not be over-emphasised when it is stated that nearly half of the engineering products are produced through machining at one stage or the other. In the age of wide spread automation, we are witnessing the trend that the demand for productivity and process optimization is increasing day by day. As the search for new materials and processes is continuing, effort is still underway to improve conventional process by reducing the material wastage to a bare minimum, increasing tool-life and improving the product finish. In view of the crucial role played by machining among all the material processing operations, a scientific understanding of various metal-cutting processes is vital for modern engineering technology and practice.

A detailed analysis of the mechanics of metal cutting which sheds light on the underlying plastic deformations, thermal phenomena and diffusion phenomena, is helpful in the prediction of cutting tool wear.

Over a past few decades, a large volume of experimental data has been collected on cutting tool wear, but a comprehensive theoretical understanding of this highly complex phenomenon is yet to emerge. In order to estimate the tool wear rate, one has to rely on empirical relations based on experimental measurements and material properties.

The present work, in its right ernest, is a small effort to fill some existing gaps in the theory of cutting tool wear. A coupled analyses of heat transfer and diffusion throughout the whole region of the work piece, chip and tool has been attempted here, to provide a reasonably accurate estimate of the tool wear.

1.2 REVIEW OF PREVIOUS WORKS

1.2.1 *MECHANICS OF CHIP FORMATION*

The earliest systematic study of metal cutting process, dates back to the end of 19th century, when pioneering researchers like *Mallock, Tresca* etc. attempted to throw some light on the mechanics of machining. However, a major contribution to this area which had an important influence on the practical development of machining was the work by *Taylor* [1907]. He was particularly concerned with tool wear and tool life and seems to be the first to recognize the influence of temperature on tool wear. He developed a relationship between tool life and the speed of

machining which is still in use today.

After this work, research in the area of metal cutting commenced from the post war period. The first attempts towards developing an understanding of the mechanics of metal cutting were performed by analyzing the chip formation process. A pioneering work was carried out by *Merchant* [1944, 1945] on the so called classical "single shear plane model". This model assumes that the chip is formed due to plastic deformation occurring along a single plane, known as the 'shear plane'. The most advantageous aspect of this model is that it enables the determination of the average yield shear stress and slip velocity along the shear plane, purely through geometric constructions. It also established beyond any doubt that metal cutting is basically a shear deformation process.

Piispanen [1948] performed an analysis similar to that of *Merchant* [1945]. He has considered the additional aspects of internal friction and strain hardening. He has shown that a high cutting speed decreases the friction angle on the face of the tool, by which the forces loading the machine tool steeply may be decreased.

Drucker [1949] investigated two dimensional orthogonal cutting in detail, introducing several concepts and hypotheses which apply equally well to the most general cutting operation. Of these the most significant is the high rate of plastic deformation process. He has explained *Ekstein*'s paradox and

correlated the influences of speed of cutting, depth of cut and rake angle by the consideration of dynamic plasticity. In addition, the effect of non-homogeneity of the material is analyzed and shown to account for the gradual change from the discontinuous to the continuous type chip as the cutting speed is increased.

The shear plane model of *Merchant* [1944, 1945] *and Piispanen* [1948] was improved by *Palmer & Oxley* [1954] and *Okushima & Hitomi* [1957]. These studies suggested that through the formation of chip occurs due to the flow of metal under shear and deformation is not limited to a single plane; it occurs in a narrow region approximated by two parallel planes. This model later came to be known as the thick shear zone model. In view of the small thickness of the shear zone in comparison to its length, this model assumes that the state of stress within the deformation region is uniform simple shear.

Around the same period of the above mentioned theoretical models, efforts were going on to validate them with experimentation . *Kececioglu* [1958] was the first person to observe the process through photo-micro graph. The plastic zone where the chip formation takes place was photographed at short intervals using a quick stop device. By noting the deformation of the grain boundaries, the size and the shape of the plastic deformation zone were estimated. This study established that the

plastic region could be approximately represented by a thin parallel-sided zone.

Later, a more effective way of using photo-micro graph technique was proposed by *Stevenson & Oxley* [1969]. Assuming a thin parallel-sided zone, they observed printed grids on the material before and after deformation. From the streamlines of metal flow, the strains and strain rates were calculated.

1.2.2 *PREDICTION OF TEMPERATURE IN ORTHOGONAL CUTTING*

Hann [1951] calculated the shear plane temperature by assuming the shear plane to be a uniform band of heat source moving obliquely through an infinite work piece.

Loewen & Shaw [1954] also assumed the shear plane to be a uniform band of heat source but considered that it moved over a semi-infinite work piece with the proportions of the shear plane heat entering the work piece and the chip determined by *Blok*'s partition principle.

Trigger & Chao [1951] used *Blok*'s [1938] partition principle to calculate the average tool-chip interface temperature assuming that the heat developed at the tool-chip interface was uniformly distributed.

Weiner [1955] obtained a solution for the shear plane temperature distribution by assuming that the chip velocity was

perpendicular to the shear plane and that the heat conduction in the direction of motion of the work piece and chip could be neglected.

Rapier [1954] calculated temperature distributions in the work piece, chip and tool which he treated as three separate systems. He also assumed a constant shear plane temperature and a plane uniform heat source at the tool-chip interface with all the heat flowing into the chip and none into the tool.

Dutt & Brewer [1964] improved the analysis by treating the work piece, chip and tool as one system, but after making some approximations found that they were able to dispense with the tool region altogether. In this way they were able determine the proportions of shear plane heat entering the chip and tool.

Chao & Trigger [1955] improved their earlier analytical solution for the interface temperature distribution by allowing the fraction of interface heat flowing into the tool to vary along the interface although still assuming a uniform heat source.

The disadvantages of the above methods of temperature calculation result from the simplifications made in the shear plane model. This assumes a velocity discontinuity along the shear plane while in real situations, the transition from the work piece to chip velocity occurs gradually over a finite plastic zone. Also the velocity of the chip material adjacent to the tool-chip interface (i.e. within the secondary zone) is less than

the chip velocity, resulting in the characteristic deformation observed in this region.

It has been assumed in all the cases that the generated heat is unifomly confined within the shear plane and the tool-chip interface rather than being spread over the finite primary and secondary plastic zones. A further disadvantage is that, with the exception of the work of *Dutt & Brewer* [1964], the shear plane & interface temperatures were calculated independently assuming that there is no interaction between the two heat sources when in fact some interaction would be expected.

1.2.3 *VISCOPLASTIC MODELS : DEFORMATION & TEMPERATURE PREDICTION USING FINITE ELEMENT METHOD*

The credit for the effective usage of the Finite Element Method (F.E.M) to viscoplastic analysis goes to *Zienkiwicz et al.* [1981]. In 1978, these researchers applied FEM for the modelling of metal forming and extrusion problems. In metal cutting, the FEM technique was employed by *Tay & Stevenson* [1974, 1976] for predicting the temperature field for orthogonal machining. They used hyperbolic streamlines in the primary deformation zone for calculating the velocity field & strain rates. They also derived semi-empirical relations for computing heat generation. However, these studies do not provide a coupled analysis of plastic

deformation and thermal processes during metal cutting.

Stevenson, Wright & Chow [1983] modified the work of *Tay, Stevenson & Davis* [1976] in calculating the temperature distributions in the chip and tool during metal cutting for an extended range of shear angles & contact lengths. They observed good agreement between their FEM results and earlier experimental measurements.

Murarka et al. [1979] predicted the temperature field variation during metal cutting and verified the average temperature rise by experimental measurements. These authors obtained the temperature distribution near the tool-tip for a wide range of cutting conditions.

Balaji et al. [1986] applied the FEM technique to evaluate the temperature field within the work material and the tool, for coated carbide tools. The effects of protective coating upon the tool-chip interface temperature, and heat transfer characteristics have been investigated in their work. They have also provided the experimental verifications of the results obtained.

Strenkowski & Carroll [1985] used FEM to predict the chip geometry, plastic deformation and the residual stresses in the work piece. They have presented an adiabatic heating model to stimulate the heat generation effects due to plastic work. But they did not consider the coupled temperature field in the tool

Strenkowski & Moon [1990] modified the work of *Strenkowski &*

Carroll [1985] by considering the temperature distribution in the work piece, chip and tool without the need of empirical cutting data.

Sarma [1990] calculated the nature of temperature distributions in the work piece and the chip during machining. He assumed that heat is generated due to plastic deformation at the primary zone and due to plastic deformation as well as frictional rubbings at the secondary zone. He considered constant values for material properties such as thermal conductivity, specific heat and yield stress.

Despande [1992] calculated the temperature distributions in the work piece and chip during machining using the similar concepts as *Sarma* [1990]. But he considered the variation of thermal conductivity, specific heat and yield stress with temperature in calculating the temperature field.

In the most recent times, *Komvopoulos et al.* [1991] have analyzed the deformation processes in metal cutting using elasto-plastic approach. They did not consider the thermal aspects of the cutting process.

1.2.4 *CUTTING TOOL WEAR*

Numerous experiments have been conducted on tool wear during the past few decades and much is still to be done. No general

laws of tool wear have been deduced so far. Since metallic wear is, in general, a complex phenomenon involving chemical, physical and mechanical processes, it is clear that a theoretical treatment of the problem of tool wear at present must be accompanied by simplifications.

Dawihl [1941], after a series of investigations on crater wear of cemented-carbide tools, concluded that mutual diffusion of materials at the tool-chip interface and the propensity to welding of certain constituents in sintered carbide with steel were of direct concern. He pointed out the importance of temperature at the tool-chip contact.

Trent [1952] proposed a new theory to account for the crater wear of cemented-carbide tools. He postulated that fused layers of alloy were formed between the steel and the free tungsten-carbide in the cutting tool material at the tool-chip interface. Wear was the consequence of the transportations of the fused alloy by the moving chip. The extent of cratering was controlled by the distribution of temperature near the cutting edge.

Trigger & Chao [1956] also found that wear at the top surface of the tool is essentially of the transfer type and formation of crater wear is strongly temperature dependent.

Cook & Nayak [1966] presented an empirical relation to show that the geometry of the tool wear is strongly controlled by the

chip curl. They presented simple theories to calculate the rate of tool wear based on diffusion of tool material into the work piece.

Rubenstein [1975] deduced an analysis of continuous flank face wear which is attributed only to adhesion between tool and work piece material. His analysis is based on the assumptions that flank face wear occurs exclusively by the adhesion mechanism and 'weld' formation occurs by a diffusion process which is temperature and time dependent.

Kannatey-Asibu [1985] derived a two dimensional transport-diffusion equation for in metal cutting, by an extension of the *Fick*'s second law of diffusion. The analysis considers the dynamics of the cutting process and thus offers a comprehensive representation of the diffusing species in the work piece and the chip.

1.3 OBJECTIVES AND SCOPE OF THE PRESENT WORK

In the present study, an attempt has been made to fill the gap in the analysis of cutting tool wear by solving the coupled heat transfer and diffusion equations.

It is well established from previous experiments that the deformation is restricted to a very small region around the tool-tip. Therefore, a solution domain extending upto a few

millimeters from the tool-tip into the workpiece and the chip has been considered. Beyond this domain, work material is assumed to be perfectly rigid. The tool is also taken to be perfectly rigid and sharp, with no built-up edge. The tool cutting edge is assumed to be orthogonal to the cutting direction. Heat generation during machining is restricted to the primary and the secondary zones only. The heat generation in the primary zone is due to plastic deformation only whereas in the secondary zone, it is due to both plastic deformation and interfacial friction.

The changes in material properties such as the specific heat, thermal conductivity and the diffusion coefficient with temperature have been taken into account, since metal cutting involves large temperature variations. Based on the temperature field within the whole domain, carbon concentration has been calculated throughout the region considering two-dimensional species-diffusion equation. The yield stress for the tool material has been assumed as a function of both the temperature and the carbon concentration. The actual shear stress which is exerted by the chip on the tool surface, varies with distance from the tool-tip. From the tool-tip to the 'sticking ' portion, it is constant and beyond that it decreses linearly to zero at the point where the chip leaves the surface. In the present work, it has been assumed that if actual surface stress is more than the calculated yield stress - erosion occurs resulting in 'crater'

wear on the rake face. Prediction of crater wear profile has been done on the basis of this assumption for two cases of cutting conditions.

A special software for FEM grid generation has been developed, since grid generation for the complex geometry encountered in the present study is quite a difficult task. Some of the advanced concepts such as the hyperbolic streamline model (*Tay et al.* [1974]) and the trans-finite interpolation have been used in the grid generation algorithm.

1.4 ORGANISATION OF THE THESIS

Chapter 1 of the thesis provides the introduction of the problem and a review of literature relevant to the basic mechanisms involved in orthogonal metal cutting which influence the temperature field around the tip and the cutting tool wear. The theoretical formulation of the problem is presented in Chapter 2. Chapter 3 details the finite element analysis of the heat transfer and diffusion equations in the vicinity of the cutting edge. Chapter 4 presents the numerical results. Comparison of the results obtained with those of the earlier researchers has been included in this chapter. Chapter 5 presents the conclusions and the scope of further research.

CHAPTER 2

THEORETICAL FORMULATION

Metal cutting involves very complex deformation phenomena. Extremely localized asymmetric deformation occurs at exceedingly high strain rates, in a minute domain of few millimeters size. The metal cutting action itself is a consequence of high compression followed by shearing of the metal. Consequently, any theoretical treatment of the metal cutting process is bound to involve certain relaxations and simplifications.

A two dimensional orthogonal cutting condition has been considered for the analysis. In fact, orthogonal cutting is a particular case of oblique cutting, with cutting edge of the tool perpendicular to the cutting velocity vector. The tool is assumed to be sharp, with no built up edge. The work material is taken to be ductile, resulting in the formation of continuous chips. The tool and the portion of the work material outside the solution domain on the other hand, are taken to be perfectly rigid without any deformation.

2.1 PLASTIC DEFORMATION & CHIP FORMATION IN ORTHOGONAL CUTTING

In orthogonal cutting, the fact that the width of the chip is large compared to its thickness, renders the problem two dimensional. Although the deformation in metal cutting is similar to those of the metal forming processes, a distinguishing feature is that the deformed material, is separated from the parent work piece in the form of a chip. Hence, it is of primary importance to analyze the chip formation process, in any theoretical analysis of metal cutting.

The uncut material in motion is first interrupted by the cutting tool, causing severe compressive stresses in the material. After sufficient compression, when the resulting shear stresses in the material attain the yield value, plastic flow of the material occurs in the direction of shear force leading to the formation of the chip. The outward shearing movement of each successive deforming element is arrested by work hardening and the movement is transferred to the next element.

It is well accepted now that the predominant mechanism of metal cutting is that by shearing process occurring in the zone called 'shear zone'. A detailed study of metal cutting reveals that two such zones exist in the domain.

(i) Primary shear deformation zone (PSDZ)

(ii) Secondary shear deformation zone (SSDZ)

These two zones have been shown in Fig.(2.1). The primary shear deformation zone has been observed to be wedge shaped and

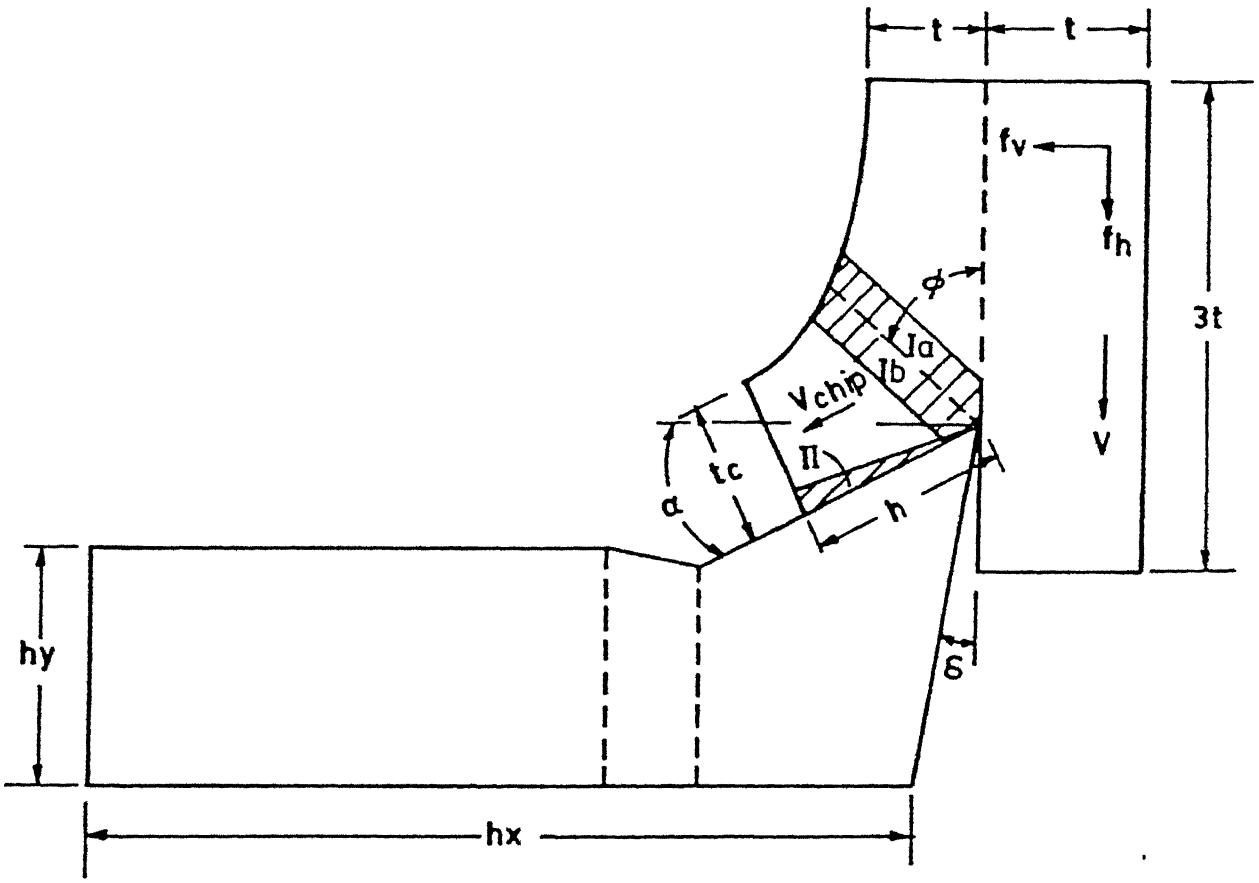

FIG. 2.1 : SHEAR DEFORMATION ZONES

its size depends upon cutting velocity. It has been reported that an increase in cutting velocity causes the thickness of PSDZ to reduce. The thickness or mean width of PSDZ is an important quantity which gives an idea of the rate of deformation and the amount of heat generated. The narrower the region, the greater the rate of deformation.

The secondary shear deformation lies adjacent to the contact patch between the chip and the tool. Additional deformation due to friction takes place here. Each layer in SSDZ moves at a different speed because of shearing in a direction parallel to the rake face of the tool. An interesting point to note is that the highest temperature occurs on the interface between the chip and the tool. The temperature in SSDZ is higher than that in PSDZ mainly due to the fact that the metal flow velocity is very low in SSDZ and also that the material which enters SSDZ has already been heated through PSDZ. Some of the researchers (*Jain et al.* [1987]) have attempted to estimate the thickness of these zones theoretically and experimentally.

2.2 GOVERNING EQUATIONS

2.2.1 *TEMPERATURE FIELD IN THE CUTTING DOMAIN*

In the present analysis, temperature fields in the plastic deformation zones of the work piece, chip and the tool during

machining are analyzed. It is obvious that in order to get a real picture of the temperature distribution in the whole region around the cutting edge, heat generation must be calculated carefully. It has been assumed that all of the work done is converted into heat, which seems to be quite reasonable because the material density does not change considerably and also, work hardening is not severe due to the high temperature conditions.

The steady state heat balance equation in the regions surrounding the cutting edge can be written in a general form

$$\frac{\partial}{\partial x}\left\{k_i \frac{\partial T}{\partial x}\right\} + \frac{\partial}{\partial y}\left\{k_i \frac{\partial T}{\partial y}\right\} - \rho_i c_{pi}\left\{u \frac{\partial T}{\partial x} + v \frac{\partial T}{\partial y}\right\} + \dot{Q}_i = 0, \qquad (2.1)$$

where T is the temperature field, u and v are the components of the velocity field, k, ρ, c_p are the thermal conductivity, density and specific heat respectively, and $\dot{Q}_i$ is the rate of heat generation per unit volume. The subcript i is used to denote different regions around the tool tip such as the fully formed chip, uncut material, machined region, PSDZ, SSDZ and the tool. It is evident that in order to solve equation (2.1), it is necessary to find out the material properties (k, ρ, c_p), the velocity field (u, v) and the rate of heat generation $\dot{Q}$ in each zone. The procedures followed to calculate each of the above quantities are detailed in the following sections.

2.2.2 *CALCULATION OF VELOCITY FIELDS*

For calculating the velocity field at different locations some approximations have been made. Within the uncut metal and fully formed chip, the velocity field is taken to be uniform given by V and V_{chip} respectively, where $V = (\pi D_1 N) / 1000$ and $V_{chip} = Vr$. In the above expression, r is the chip thickness ratio given by $r = t/t_c$

In the primary zone (I) and the secondary zone (II) (Fig. (2.1)) where plastic deformation takes place, velocity varies from location to location. For the primary zone the velocity at any location is obtained by linearly interpolating between the values V and V_{chip}. The primary zone is divided into two layers of equal thickness for the sake of velocity calculation. The elements in the first row (I_a) have velocity components of the form :

$$\left.\begin{aligned} u &= -(V_{chip} \cos\alpha) / 3. \\ \text{and,} v &= -(2.V + V_{chip} \sin\alpha) 3. \end{aligned}\right\} \qquad (2.2\ a,\ b)$$

The elements in the second row (I_b) have velocity components given by :

$$\left.\begin{aligned} u &= -(2\ V_{chip} \cos\alpha) / 3. \\ \text{and,} v &= -(V + 2\ V_{chip} \sin\alpha) / 3 \end{aligned}\right\} \qquad (2.3\ a,\ b)$$

The velocity components in the fully formed chip are :

$$\left.\begin{aligned} u &= -V_{chip} \cos\alpha \\ \text{and,}\quad v &= -V_{chip} \sin\alpha \end{aligned}\right\} \qquad (2.4\ a, b)$$

The components of the metal flow velocity in the secondary zone depend upon the sliding velocity of the chip at the interface. *Tay et al.* [1976] found that the sliding velocity of the chip at the interface is given approximately by the equation -

$$V_{int} = \frac{1}{3} (V_{chip}) \sqrt{(1 + (8\ x)\ /h)}, \qquad (2.5)$$

where 'x' is the distance from the cutting edge measured along the interface and 'h' is the total contact length.

For calculating the velocity field in the secondary zone, linear interpolation is used between the chip velocity (V_{chip}) and the interfacial velocity (V_{int}) similar to that in the primary zone. In the tool region, the velocity components u and v are taken to be zero.

2.2.3 *HEAT GENERATION DURING MACHINING*

The rate of heat generation per unit volume is assumed to be zero everywhere except in the primary and secondary deformation zones.

Heat generation in the primary shear deformation zone is due to plastic work only. The rate of heat generation (per unit volume) $\dot{Q}_{pz}$ at any point in the primary zone is given by

$$\dot{Q}_{pz} = (fs\ vs) / volume1, \tag{2.6}$$

where fs, vs and volume1 are the shear force, shear velocity and volume of the primary deformation zone respectively. Here, shear force can be calculated using *Merchant*'s circle diagram (see, Fig. (2.2)), using the expressions :

$$fs = fh \cos \phi - fv \sin \phi$$

$$\text{and, } vs = V \cos \alpha / \cos(\phi - \alpha),$$

where V, ϕ and α are the cutting velocity, shear angle and rake angle respectively. Volume of the primary deformation zone is given as the product of the 'width of cut' and the area of PSDZ.

In the secondary shear deformation zone, there are two types of heat generation. One is due to the secondary plastic work and the other is due to the interfacial friction. Upto to the point of 'sticking friction' both types of heat generation are present, whereas beyond the point of sticking friction only frictional heat generation is present. Shear stress is constant in the sticking friction point and after that it varies linearly with rest of the

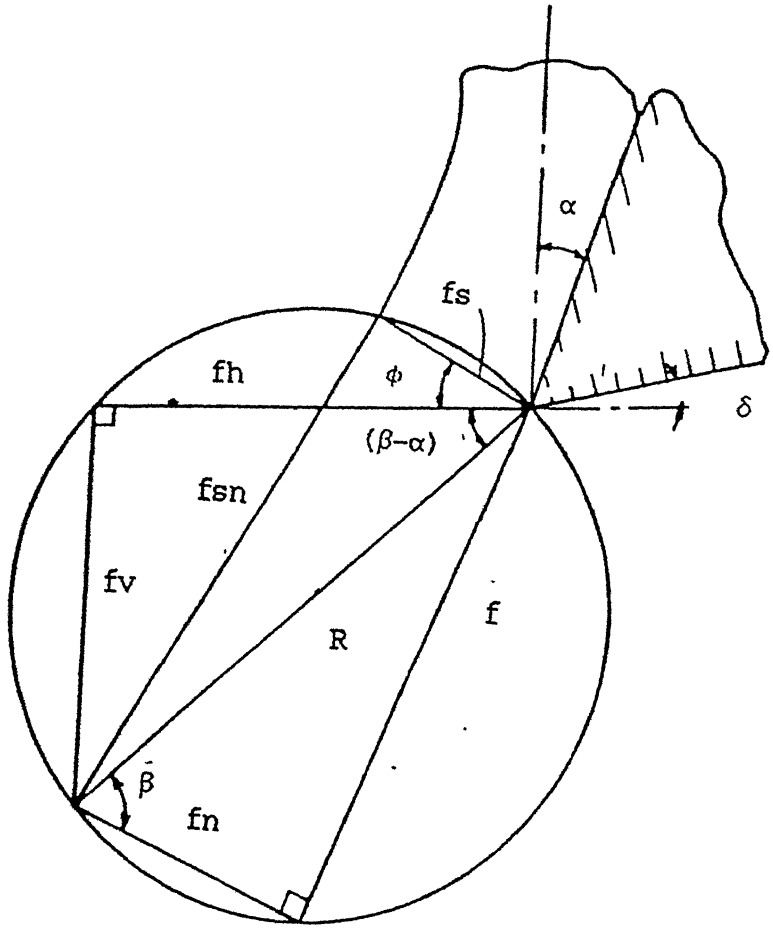

FIG. 2.2 : MERCHANT'S CIRCLE DIAGRAM FOR FORCES

contact length and becoming to zero at the point where the chip leaves the tool rake surface (see, Fig. (2.3)).

Heat generation due to secondary plastic work is given by

$$\dot{Q}_{2a} = f2a\ (V_{chip} - V_{int}) \ /\ delta2\ (1 - x\ /h), \qquad (2.7a)$$

where f2a, h and delta2 are the shear stress, the contact length and the thickness of the secondary deformation zone respectively. Also, x is the distance from the cutting edge along the contact length. Here, the SSDZ is assumed to be of triangular in shape (*Tay et al.*[1976]), consisting of one layer of elements adjacent to the rake face within the chip. Its maximum thickness delta2 has been taken as :

$$delta2 = (0.154\ t) \ /\ \sin \phi \qquad (2.7b)$$

Heat generation due to frictional work $\dot{Q}_{2b}$ has been calculated as follows

$$\dot{Q}_{2b} = f2b\ V_{int} \ /\ delta2\ (1 - x\ /h), \qquad (2.8)$$

where f2b and V_{int} are the shear stress and the interfacial velocity (see, equation (2.5)) respectively.

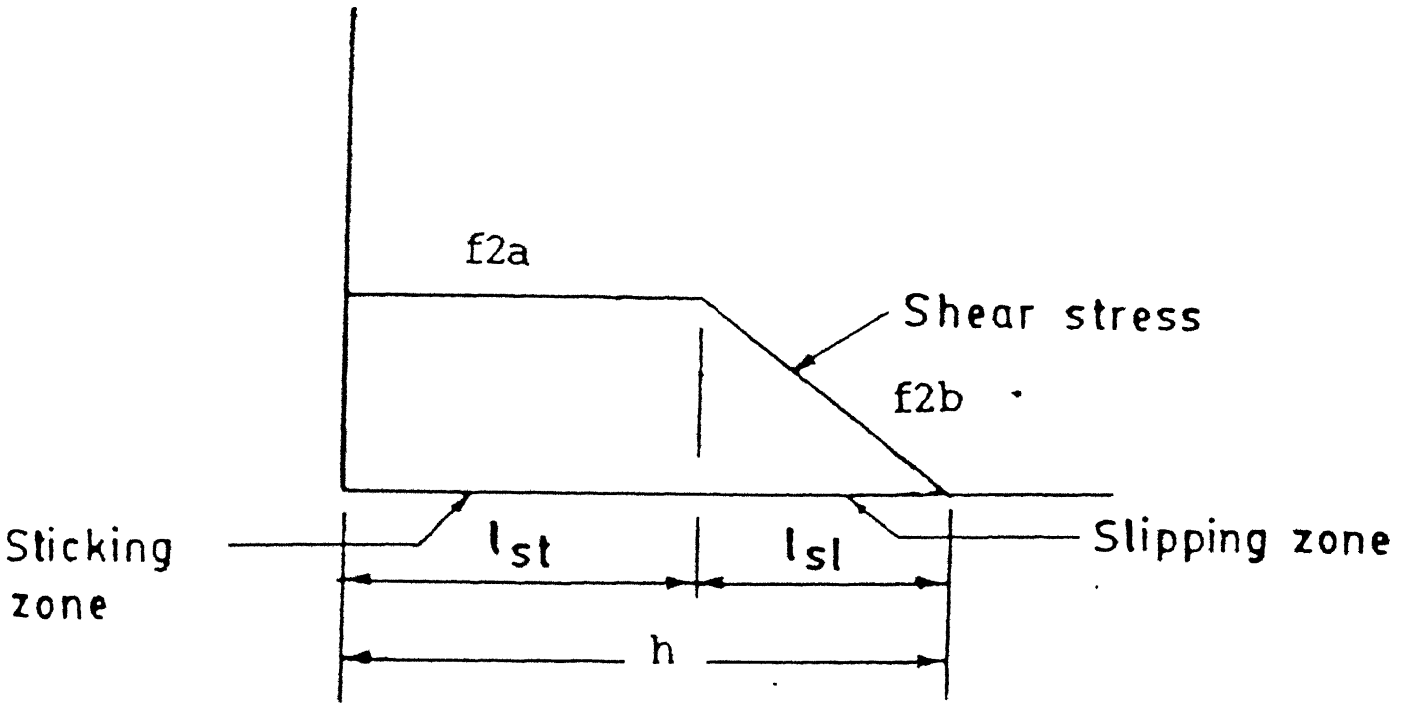

FIG. 2.3 : VARIATION OF SHEAR STRESS ON THE RAKE FACE OF THE TOOL

2.2.4 *EVALUATION OF THERMAL PROPERTIES*

A careful study of the governing equations reveal that the material properties such as thermal conductivity and specific heat affect the temperature solution to a considerable extent. All the above mentioned properties vary with temperature. In particular, at high temperatures, the variations become quite significant.

In the present analysis, the solution domain is a minute region surrounding the tool tip. As already mentioned elsewhere, the temperatures in this region are quite high due to the rate of plastic deformation. Thus, to have a realistic picture of the results, the variations in these properties at higher temperatures are incorporated in the analysis, where material data is available.

The variation of the thermal conductivity and the specific heat are curve fitted and property correlations have been derived. For thermal conductivity and specific heat , piece wise equations of a straight line of the type $y = mx + c$ have been fitted for different temperature ranges. The data used in the present study is shown in Figs. ((2.4), (2.5) and (2.6)).

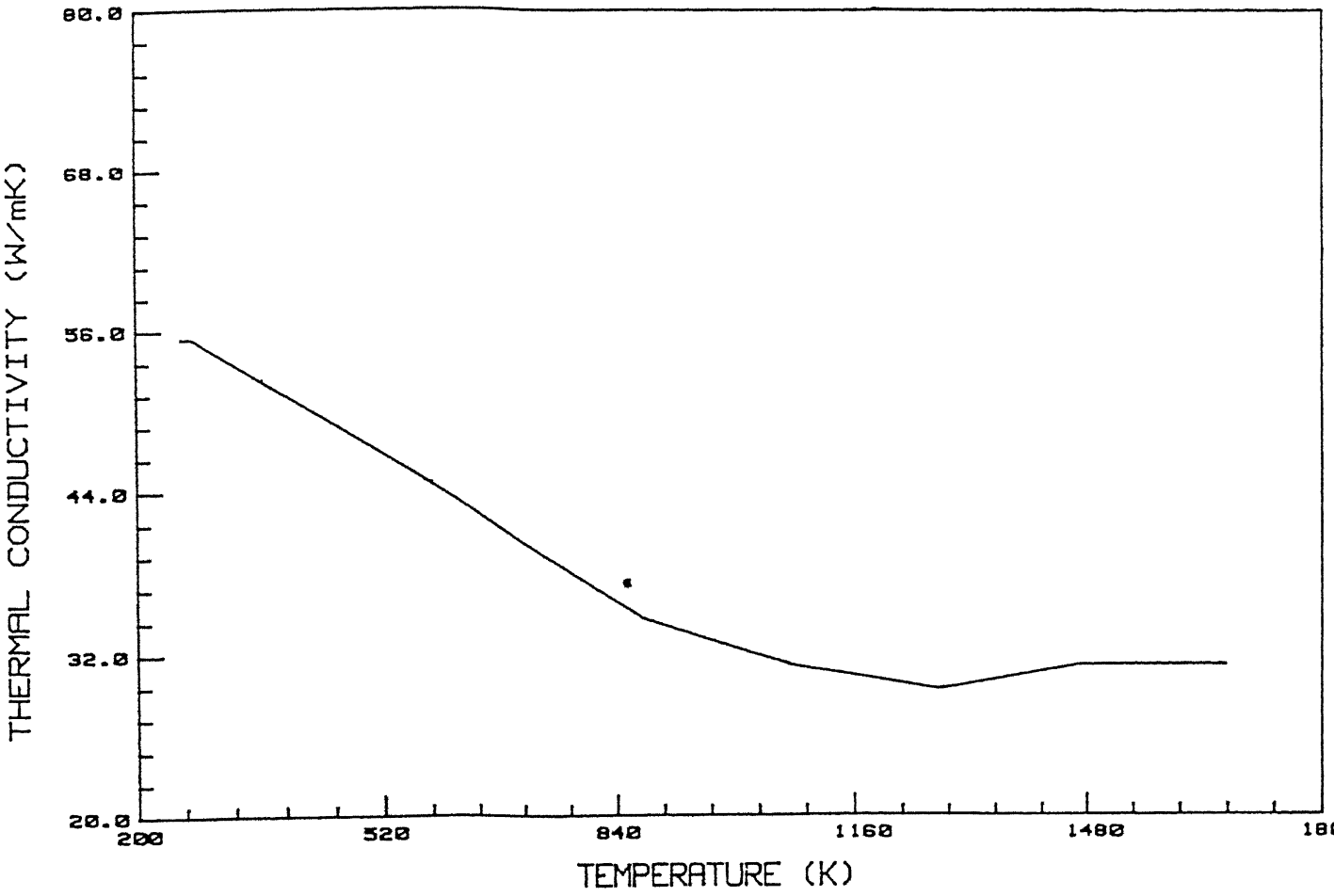

FIG 2.4 : VARIATION OF THERMAL CONDUCTIVITY WITH TEMPEARTURE IN WORKPIECE (MILD STEEL)

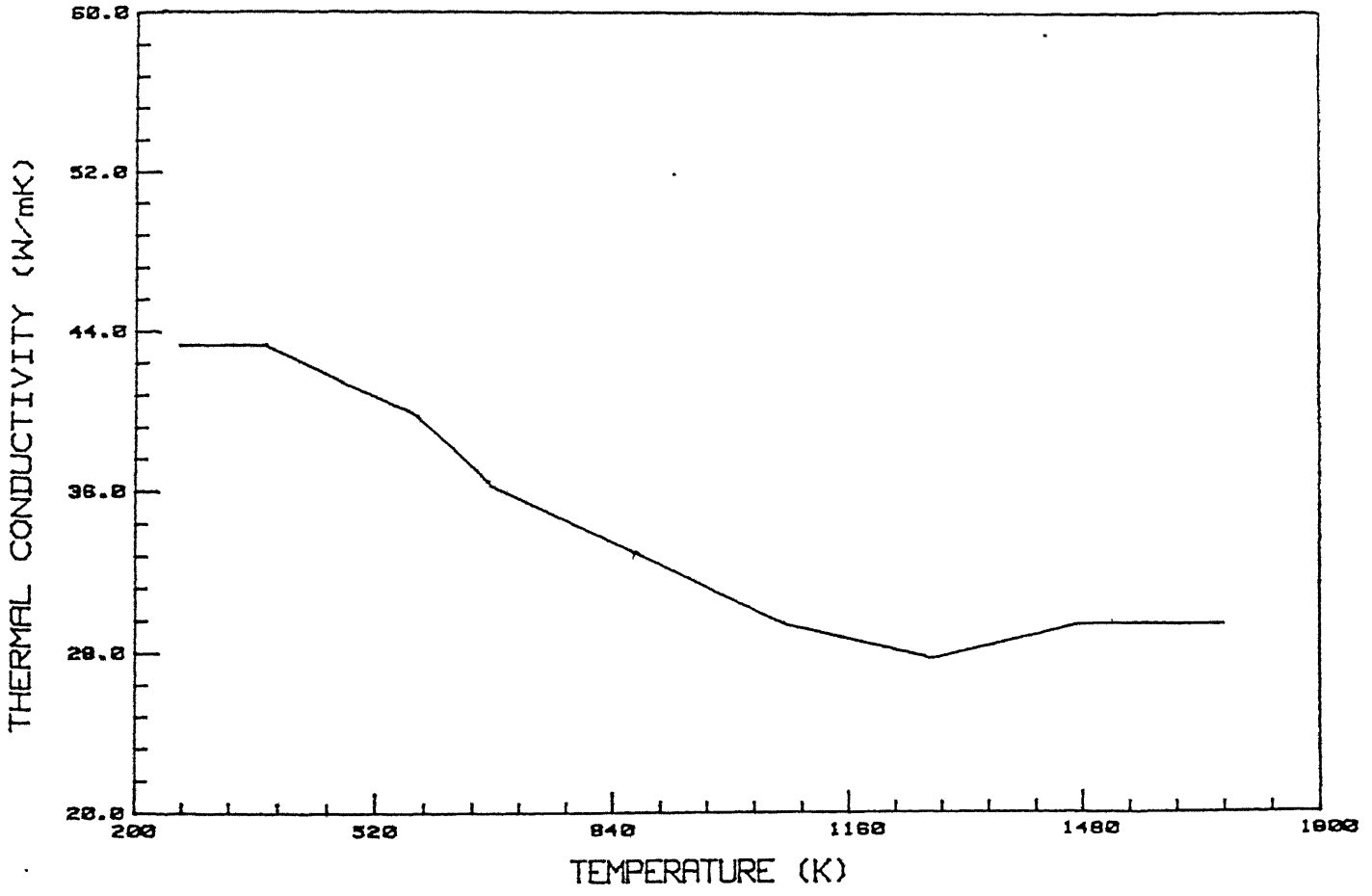

FIG 2.5 : VARIATION OF THERMAL CONDUCTIVITY WITH TEMPEARTURE IN TOOL (HIGH SPEED STEEL)

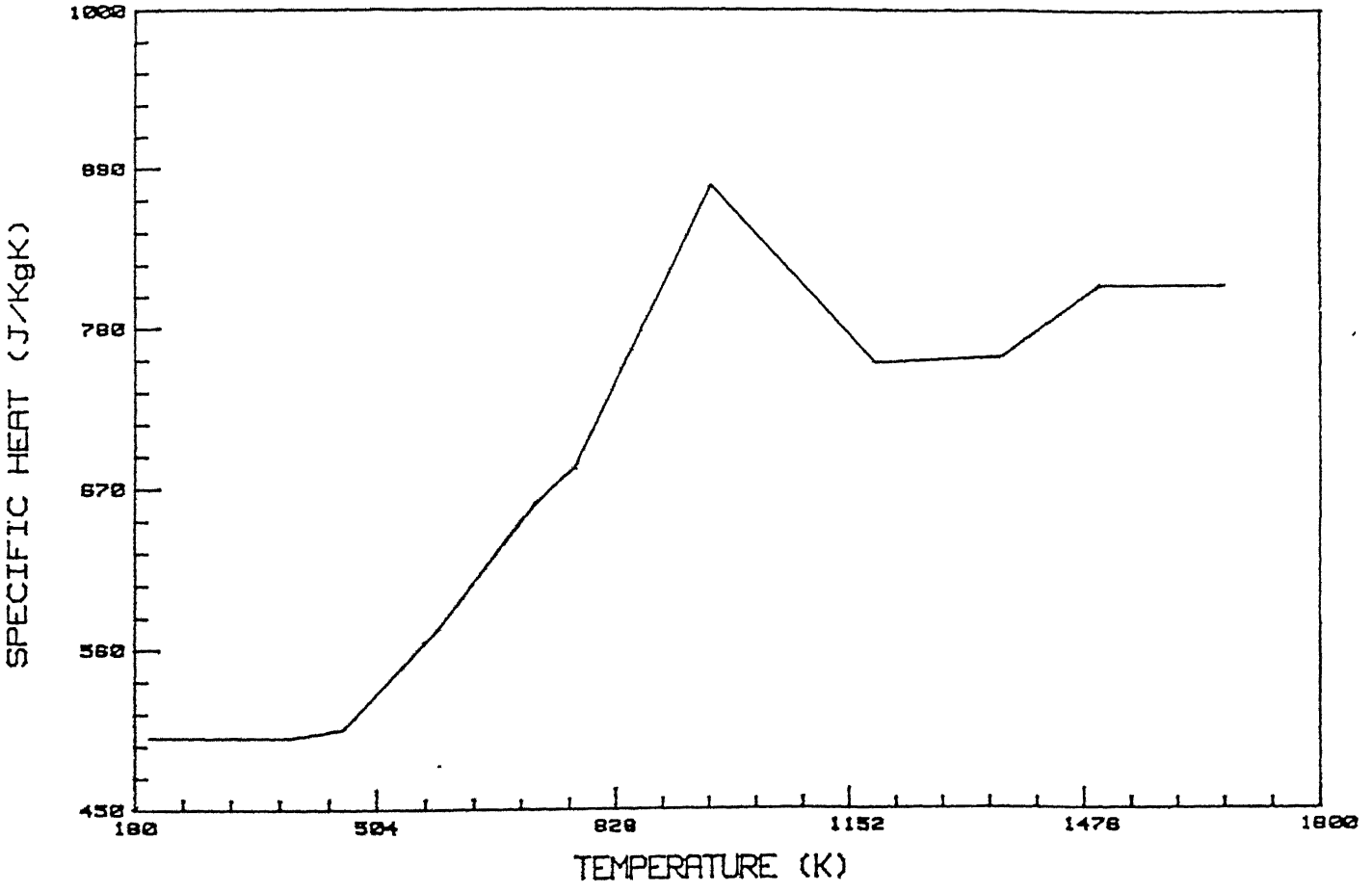

FIG. 2.6 : VARIATION OF SPECIFIC HEAT WITH TEMPERATURE IN WORKPIECE (MILD STEEL)

2.3 ANALYSIS OF TOOL WEAR

A cutting tool may fail because of any one of the mechanisms such as the process of softening due to plastic deformation, brittle fracture due to mechanical loads, shocks and gradual wear.

The failure due to plastic deformation of the cutting edge takes place when the hardness of the cutting edge is not sufficient to maintain the original shape of the tool. The stresses developed because of the resistance of the work material at the prevailing temperature and strain rate cause rounding of the cutting edge. According to *Bhattacharya & Sen* [1984], it has been shown that if the ratio between the hardness of the tool and the chip material exceeds 1.5, such failures are not expected.

Failures by brittle fracture are due to excessive pressure and load or shocks such are present in intermittent cutting, quick freezing of the cutting action, cutting under chatter condition, etc. However, brittle fractures are avoidable by proper selection of cutting conditions (feed, depth of cut, etc.) or by strengthening the cutting edge with a land.

But still, cutting tools continue to fail by a process of wear which is due to the interactions between the chip and the tool or between the work piece and the tool. After the cutting has progressed for some time, wear which appears on the tool face because of tool-chip interaction, forms a cavity known as

'crater'. It begins at a certain distance from the cutting edge. On the other hand, wear which takes place due to the rubbing of the tool with the work piece on the flank face of the tool is known as 'flank wear'.

2.3.1 *MECHANISM OF WEARING PROCESS*

Wear is not a process involving one unique mechanism — there are several mechanisms which are known to be operative, depending on the physical conditions existing. Four main wear mechanisms have been identified as follows :

(1) Adhesion

(2) Abrasion

(3) Diffusion

(4) Fatigue

(1) *Adhesion Wear* : Due to the existance of a very high temperature region on the chip-tool interface, formation of temporarily welded junctions between the tool and the chip and the subsequent destruction of these occurs continuously. When the destruction is by shearing below the interface, a wear particle is transferred. This mechanism is termed as the adhesion wear.

(2) *Abrasion Wear* : The abrasion process involves cutting at the microscopic level and as such, it depends on the hardness, the elastic properties and the geometry of the two mating surfaces.

It has been pointed out that the larger the amount of elastic deformation a surface can sustain, the greater will be its resistance to abrasion.

(3) *Diffusion Wear* : Holm proposed diffusion wear as a process of atomic transfer at contacting asperities which eventually causes material softening leading to wear. It is a highly temperature-dependent phenomenon, i.e., a direct function of the rubbing speed. However, the amount of material transferred by diffusion is also dependent on the time of contact of the mating surfaces, which is an inverse function of speed.

(4) *Fatigue Wear* : This is described as the process of change in stress in the material below a surface as an asperity from a rubbing surface passes over it. Each asperity is associated with a wave of deformation. At some distance ahead of the asperity the underlying material is compressed, but behind the asperity, tensile stress elongates the material. This chamge in sign of the stress as an asperity passes a given point causes fatigue failure of the material below the surface.

In the present study, tool wear caused by the diffusion mechanism alone has been studied. The other mechanisms have been neglected for the sake of simplicity.

2.3.2 *DIFFUSION WEAR PHENOMENA*

The fact that the workpiece and tool materials are different from each other causes diffusion of carbon and other alloying elements from one material to the other. This mass transfer occurs in both the directions. Close investigation near the tool-chip interface has revealed that :

(1) There is constant migration of carbon from tool to chip. Since the carbide phase is responsible for tool hardness, carbon diffusion reduces the tool strength.

(2) There are thermal gradients in both the tool and the chip. However, because the thermal diffusivity is many orders larger than the mass diffusivity, transient variation of mass concentration needs to be considered while the temperature field can be treated as steady.

(3) The strength or hardness of materials is dependent on gross carbon diffusion and on the average, its value is higher in tool than in workpiece.

Various factors which influence the diffusion wear are :

(A) *GROSS TOOL HARDNESS* : If at the operating temperature, the tool is soft enough that the interfacial stresses cause gross deformation, the tool geometry will clearly deteriorate. This imposes a hardness criterion on the tool material which may be separate and distinct from a wear criterion. In steel tools, this mechanism can inhibit cutting due to diffusion-controlled carbon depletion of a relatively deep surface layer or to 'annealing' in

which the carbon diffusion permits a change in crystal structure.

(B) *GROSS DIFFUSION OF TOOL INTO THE WORK PIECE* : In this mechanism, the tool matrix material, or a major strengthening component, is dissolved by the chip & work surface as they flow past the tool. The mechanism is somewhat analogous to the dissolution of a salt crystal in a moving stream of water. This effect could be present in carbide tools with carbon diffusing from the WC into the work. In cast alloys and ceramics, this could be predominant. In steel tool, it is possible that the iron could diffuse into the work, if the work material is non-ferrous.

(C) *DIFFUSION OF MINOR TOOL CONSTITUENTS INTO THE WORK* : Here, a minor (but strengthwise important) component of the tool material diffuses into the work, leaving a thin surface layer with degraded physical properties. In tungsten carbide tools, cobalt which serves as the binding material could diffuse away, leaving the relatively fragile WC structure to break away. In steel tools, the carbon could diffuse away, forcing an alteration of crystal structure in a very thin surface layer.

(D) *DIFFUSION OF WORK MATERIAL COMPONENTS INTO THE TOOL* : Here, either the work material or an additive element may diffuse into a superficial tool layer, altering its physical properties. It is well known, for instance, that many liquid metals (gallium, mercury, lead & so on) produce very strong embrittling effects on other materials. It is conceivable that a work additive such as

lead could diffuse into the tool surface, rendering a surface layer quite brittle.

2.3.3 *TRANSPORT DIFFUSION EQUATION IN METAL CUTTING*

The cutting process is two dimensional for orthogonal cutting, involving bulk motion of material in the direction of diffusion as well as in a direction perpendicular to it. Taking into consideration both the process of diffusion and the bulk motion, the equation governing the transient variation of the diffusing species can be written in the form

$$\frac{\partial c}{\partial t} = \frac{\partial}{\partial x}\left(D \frac{\partial c}{\partial x}\right) + \frac{\partial}{\partial y}\left(D \frac{\partial c}{\partial y}\right) - \left(u \frac{\partial c}{\partial x} + v \frac{\partial c}{\partial y}\right), \qquad (2.9)$$

where, c is the concentration and u, v are the components of cutting velocity. These velocities are calculated in a similar way as was done for the evaluation of the temperature-field during machining.

For solid media, the diffusion coefficient (D) varies with temperature in a form given by

$$D = D_0 \exp\left(-\frac{q}{RT}\right), \qquad (2.10)$$

where, D_0 is the pre-exponential constant, q is the activation

energy for diffusion and R is the absolute gas-constant. During computation, the values of $D_0 = 0.7 * 10^{-7}$ m^2 /sec and q = 157 KJ/mol were used for both HSS and carbide tools.

It is possible to obtain the concentration field of any diffusing species, by solving equations (2.9) and (2.10). It would then be of interest to predict the deterioration in tool strength based on the temperature and concentration fields, and analyse its effects on tool wear.

2.4 SELECTION OF THE SOLUTION DOMAIN FOR ANALYSIS

It is well established from previous experiments that the deformation is restricted to a very small region around the tool tip. Therefore, a solution domain extending up to a few millimeters from the tool tip into the work piece, tool and the chip has been considered. Beyond this domain, the material is assumed to be perfectly rigid. The tool is also taken to be perfectly rigid and sharp with no built up edge. The tool edge is assumed to be orthogonal to the cutting direction. Further, for generating the domain & the finite element mesh easily, the boundary of the domain has been divided into ten surfaces, as shown in Fig. (2.7).

Surface I is the top portion of the tool extending from the tool shank to the end of contact length.

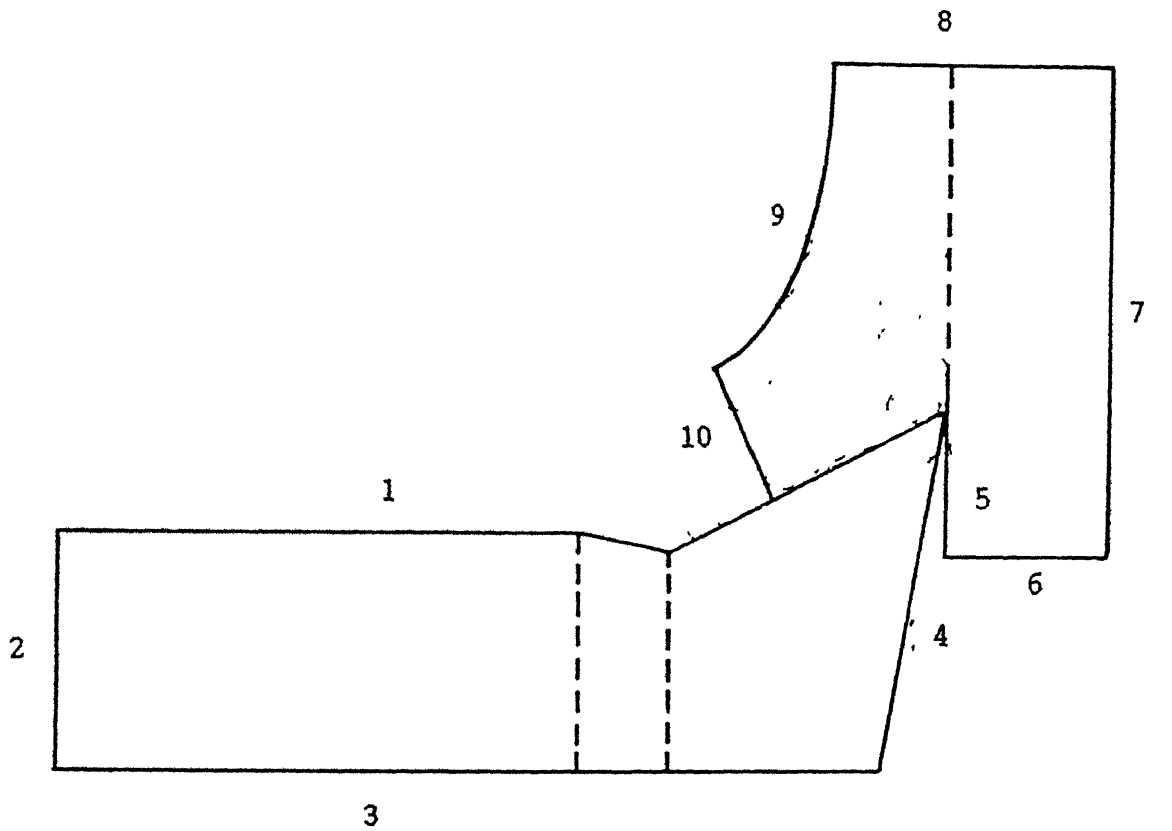

FIG 2.7 : BOUNDARY CONDITIONS OF THE SOLUTION DOMAIN

Surface II is the portion of the tool where it is clamped.

Surface III is the bottom portion of the the cutting tool.

Surface IV is the flank face of the cutting tool. Since the tool edge is sufficiently sharp and the clearance angle is adequate, there is no contact of the flank face with the machined portion of the work.

Surface V constitutes the machined surface and is exposed to the atmosphere due to the clearance angle of the tool.

Material leaves the plastic zone at surface VI.

Surface VII is selected in a plane parallel to the cutting velocity and restricts the boundary of the plastic zone below the depth of cut.

Surface VIII is the entry section where material enters the plastic solution domain and is considered to be plane, perpendicular to the cutting velocity.

The free surface of the chip, where the complex chip curling effect with serrations is observed, has been modeled using the hyperbolic stream line concept as used by *Tay et al.* [1976]. This forms the surface IX.

The chip is considered to be bounded by a plane parallel surface beyond the contact point, which is represented by surface X.

2.5 BOUNDARY CONDITIONS

2.5.1 *TEMPERATURE FIELD*

Referring to Fig. (2.7), on surfaces (2), (3), (6), (7), (8) the temperature is prescrlbed as that of the ambient. The other surfaces ((1), (4), (5), (9), (10)) have convective boundary condition which is expressed as

$$-k \frac{\partial T}{\partial n} = h'(T - T_{amb}),$$

where h' is the film heat transfer coefficient and n is the normal coordinate for the surface under consideration. The value of h' has been chosen as 50 w/mK while T_{amb} is set equal to 293 K.

2.5.2 *CONCENTRATION FIELD*

Surfaces (2), (3) have a concentration of carbon is equal to 0.85 % and surfaces (7) and (8) have carbon concentration is equal to zero (see, Fig. (2.7)). For other surfaces, the mass transfer boundary condition has been taken as

$$-D \frac{\partial c}{\partial n} = 0,$$

which implies that these surfaces are impervious (zero flux).

2.6 INITIAL CONDITIONS

The initial condition of temperature field for the tool, workpiece and the chip has been taken as that of ambient temperature.

Initial condition of concentration field for the tool has been set equal to 0.85 % and for the workpiece and the chip it is taken as 0 %.

2.7 WEAR PREDICTION

The governing equations for the temperature and concentration fields (equation (2.1) and (2.9)) have been solved numerically using the finite element method, in the present work. From the predicted temperature and concentation fields, changes in strength (yield stress) have been estimated for the tool material at each location. Eventually, based on these data, the expected tool wear profiles have been predicted. The procedure for estimating the wear profile is discussed below.

In the present work, it has been assumed that carbon is the only diffusing component from the tool to the workpiece. Although this is too simplified a picture for realistic predictions, all the important diffusing components can be taken into consideration in a similar fashion. For HSS tools, the influence of carbon concentration on tool hardness (standard Rockwell C) has been

provided in graphical form by *Clark et al.*[1987] (see Table (2.1)). It is well known that the hardness depends on the temperature also. The data for the effect of temperature on the hardness has been obtained from *Hoyle* [1988] (see Table (2.2)), for M_2 type HSS tools. Finally, the hardness at any temperature and carbon concentration has been obtained in the form

$$H(t,c) = h(T) * f(c), \tag{2.11}$$

where f(c) is a function whose value is between 0 and 1. For C > 0.60%, f(c) = 1.0. The function h(T) gives the variation in the Rockwell C hardness with respect to the tepmerature at a standard carbon concentration of 0.85%. Using standard tables for steels, (*Clark et al.*[1987], see Table (2.3)) the Rockwell C hardness has been converted into equivalent tensile strength (σ_{TS}). Finally, the yield strenght in shear (σ_{TS}) has been estimated as :

$$\sigma_{YS} = \sigma_{TS}/\sqrt{3} \tag{2.12}$$

The variation of the actual shear stress on the tool face was presented in Fig. (2.3). By comparing the yield stress with the actual surface stress, it is assumed that wear is likely to occur whenever yield stress is less than he actual stress, at any location, on the chip-tool interface. In this manner, the length

of the crater on the tool surface is approximately predicted.

The numerical solution procedure and the results obtained for some typical machining conditions are presented in the subsequent chapters.

Carbon concentration (% c)	Factor, f(c)
0.1	0.6
0.2	0.6293
0.3	0.7846
0.4	0.8769
0.45	0.923
0.5	0.9615
0.55	0.9846
0.6	1.0
0.7	1.0
0.75	1.0
0.8	1.0
0.85	1.0

· TABLE 2.1 : EFFECT OF CARBON CONCENTRATION ON HARDNESS

Temperature (K)	Hardness, h(T)
321.0	65.0
368.0	63.8
588.0	62.0
698.0	60.0
813.0	57.0
923.0	47.0

TABLE 2.2 : EFFECT OF TEMPERATURE ON HARDNESS

Standard Rockwell C (at 150 kg)	Tensile Strength (N/mm^2)
59.2	2269.68
58.7	2228.29
57.3	2131.70
50.3	1703.98
45.7	1497.02
40.4	1296.96
37.9	1214.17
34.3	1103.79
32.1	1034.81
30.9	1000.3
27.6	917.53
22.8	814.05
20.5	765.751
17.5	724.36
15.2	689.87
12.7	655.37
10.0	620.88
9.0	613.98
6.4	586.39
4.4	558.79
0.9	524.30

TABLE 2.3 : CONVERSION OF HARDNESS TO TENSILE STRENGTH

CHAPTER 3

FINITE ELEMENT ANALYSIS

3.1 INTRODUCTION

The finite element technique, whose birth and boom in the 1960*s* was due to the application of digital computers in structural analysis, has spread to a variety of engineering & physical science disciplines in the last two decades. In many engineering problems, it is not always possible to obtain a closed form exact solution. Thus, for such difficult problems, it is possible to get the best approximate solution (i.e. very close to the exact one), using a powerful numerical technique such as the finite element method.

The basic concept of finite element method is that of converting a continuous field problem into an approximately equivalent discretized problem. A finite number of points are identified in the problem domain and the values of the field variable to be solved (and its appropriate derivatives) at these points are selected as unknown variables. The points are called as nodes. The domain of the function is represented approximately by a finite collection of sub - domains called elements, which are

connected together. The solution variable is approximated locally within each element by continuous functions that are uniquely described in terms of nodal point values associated with the particular element. The path to the solution of a finite element problem consists of essentially five specific steps :

(i) integral formulation of the problem,

(ii) discretization & definition of the elements,

(iii) establishment of the nodal equations for one element,

(iv) assemblage of elemental contributions to nodal equations and incorporating boundary conditions, and

(v) the numerical solution of the global matrix equations.

The formation of nodal equations can be done using any one of the procedures such as the direct approach, variational method, method of weighted residuals, and the energy balance approach.

In the present analysis, the Galerkin's weighted residual method has been used because of its versatility.

3.2 APPLICATION OF FEM

3.2.1 *GRID GENERATION*

The first step in the finite element method is the selection of solution domain and its discretization. The choice of the solution domain boundaries for the metal cutting problem was discussed in the previous chapter. Grid generation for such a

domain is quite a tedious task. This is in view of the that the variations in depth of cut, chip thickness, rake angle or contact length, lead to totally different shapes for the solution domain. Thus, it is obvious that unless one has an efficient way of generating grid, the analysis can not be done conveniently. Grid generation, therefore, forms one of the important aspects of the present analysis.

Coordinate data and nodal connectivity of elements for each zone are calculated separately first and global element and nodal numbers for all zones are assigned later. To begin with, the coordinates for all the boundary nodes are prescribed suitably and then using a special type of interpolation technique (known as the trans-finite interpolation) coordinate data of interior points have been generated. This technique is based on transforming an arbitrary 4-sided domain into a square-domain, in terms of body-fitting coordinates (ζ, η) as shown in Fig.(3.1).

The procedure for generating the X and Y coordinate values for a typical point H is illustrated in the figure. The domain ABCD is mapped onto a unit square in the transformed (ζ, η) plane. If 'H' is the intersection point of the grid lines PQ & RS (which are η = constant, and ζ = constant lines respectively), by bi-directional interpolation, the X & Y co-ordinate of H can be obtained in terms of the X & Y co-ordinates of the boundary points P, Q, R, & S. For instance, if ζ and (1 - ζ) are the distances of

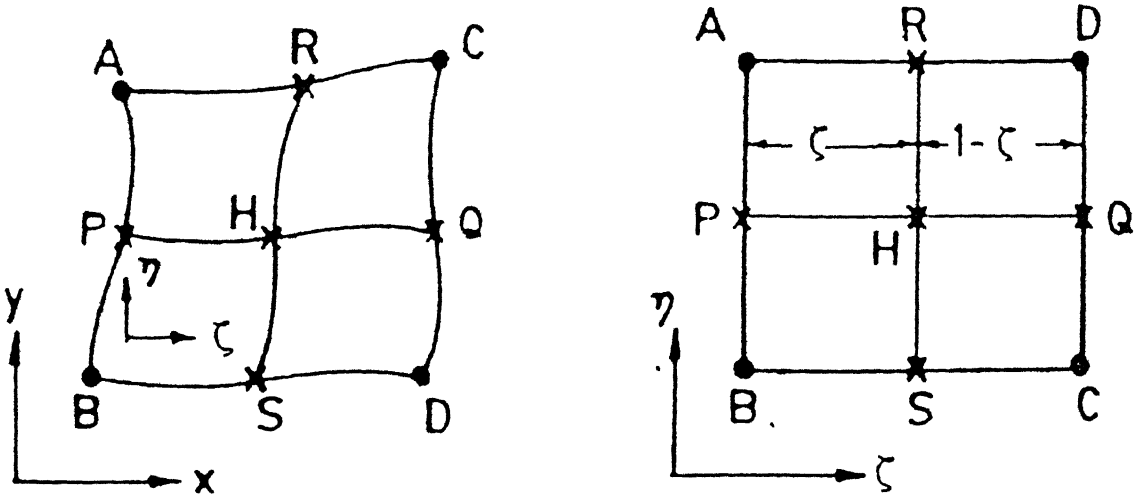

FIG 3.1 : BODY-FITTING COORDINATE TRANSFORMATION

H from P and Q respectively in the transformed domain, then for one-dimensional interpolation :

$$X_H = (1-\zeta)\, X_P + \zeta\, X_Q \qquad (3.1a)$$

$$Y_H = (1-\zeta)\, Y_P + \zeta\, Y_Q \qquad (3.1b)$$

However, for two directional interpolation, the interpolations must be applied in both ζ and η directions suitably and (X_H, Y_H) are then obtained in terms of the coordinates of the boundary points P, Q, R & S. Similarly, for obtaining the coordinates of all the interior points, the appropriate boundary points on the 4 sides are selected and by trans-finite interpolation, the interior coordinates are generated. A typical mesh thus generated, is shown in Fig. (3.2).

In the present analysis, a grid with 678 nodes and 604 elements has been used, after the observation that a smaller number of elements is not sufficient to accurately represent the sharp variations in the temperature and concentration fields. Provision has been kept in the program, to change the number of elements and the size of the elements as desired, to overcome such problems.

3.2.2 *DERIVATION OF FINITE ELEMENT EQUATIONS*

(i) *ENERGY EQUATION*

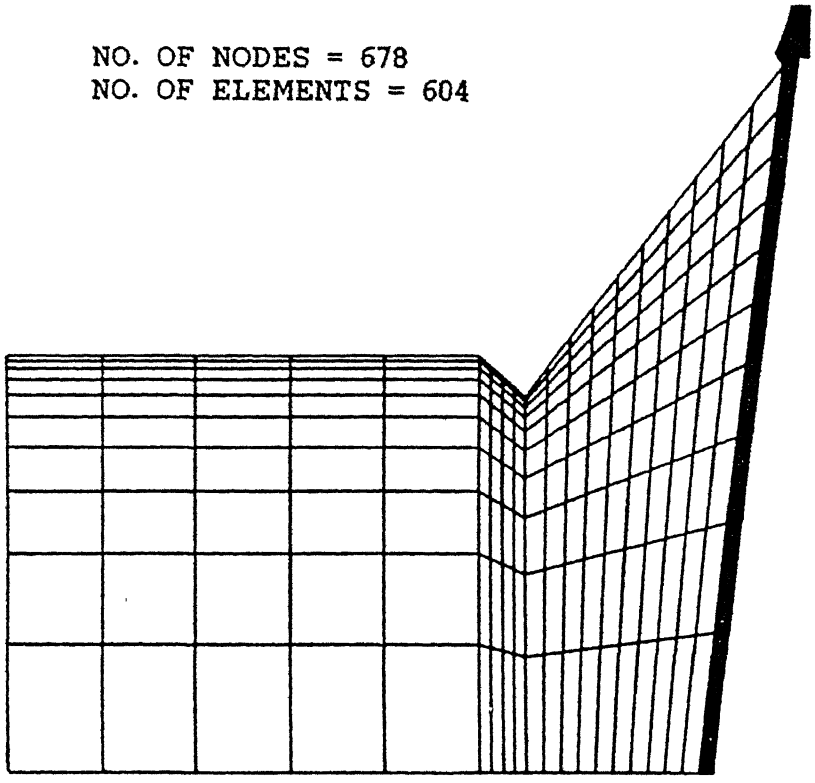

(a) OVERALL MESH

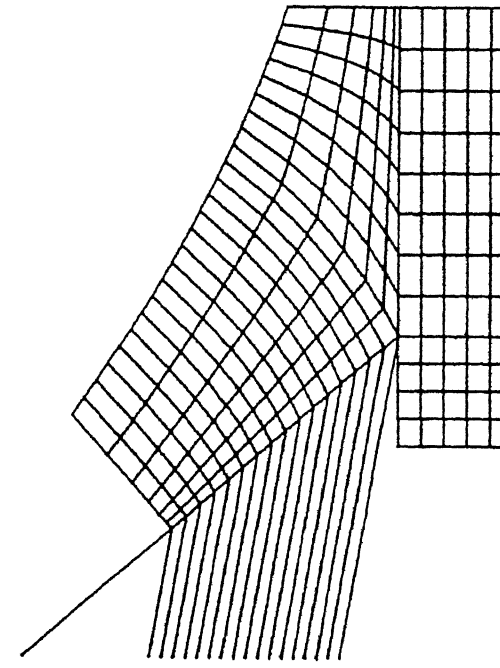

(b) MESH NEAR THE CUTTING EDGE

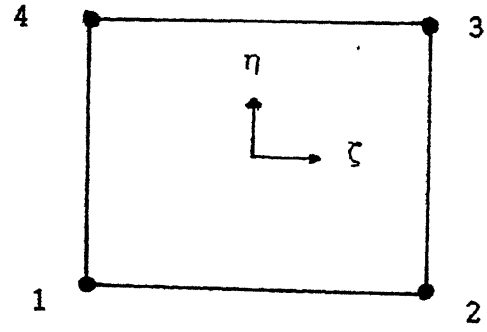

FOUR NODED ELEMENT SHOWING THE LOCAL COORDINATE SYSTEM

FIG 3.2 : SAMPLE GRID PRODUCED BY MESH GENERATOR

The two dimensional heat transfer equation was presented in the previous chapter as :

$$\frac{\partial}{\partial x}\left(k\frac{\partial T}{\partial x}\right) + \frac{\partial}{\partial y}\left(k\frac{\partial T}{\partial y}\right) - \rho\, c_p\left(u\,\frac{\partial T}{\partial x} + v\,\frac{\partial T}{\partial y}\right) + \dot{Q} = 0 \qquad (3.2)$$

In order to obtain a discretized solution, the temperature at any point within the region can be approximated as :

$$T^{(e)} = \{N\}\,\{T\}^{(ne)},$$

where $\{N\}$ is the shape function array which depends upon the coordinates and $\{T\}^{(ne)}$ is the nodal temperature vector.

The residue at a point can be written as,

$$R^{(e)} = \frac{\partial}{\partial x}\left(k\frac{\partial T^{(e)}}{\partial x}\right) + \frac{\partial}{\partial y}\left(k\frac{\partial T^{(e)}}{\partial y}\right) - \rho\, c_p\left(u\,\frac{\partial T^{(e)}}{\partial x} + v\,\frac{\partial T^{(e)}}{\partial y}\right) + \dot{Q} \qquad (3.3)$$

Now by Galerkin's weighted residual technique (*Reddy* [1986]), the equation for the i^{th} node is obtained as

$$\int\int N_i R^{(e)}\,dx\,dy = 0, \qquad (3.4)$$

where N_i is the shape function corresponding to node i. Now we can write :

$$\iint N_i \left[\frac{\partial}{\partial x}\left(k\frac{\partial T}{\partial x}^{(e)} \right) + \frac{\partial}{\partial y}\left(k\frac{\partial T}{\partial y}^{(e)} \right) - \right.$$

$$\left. \rho\, c_p \left(u\, \frac{\partial T}{\partial x}^{(e)} + v\, \frac{\partial T}{\partial y}^{(e)} \right) + \dot{Q} \right] dx\, dy = 0 \qquad (3.5)$$

Applying Green's theorem, the above equation reduces to the form :

$$\iint \left[k\left(\frac{\partial N_i}{\partial x}\frac{\partial N_j}{\partial x} + \frac{\partial N_i}{\partial y}\frac{\partial N_j}{\partial y} \right) + \rho\, c_p N_i \left(u\, \frac{\partial N_j}{\partial x} + v\, \frac{\partial N_j}{\partial y} \right) \right] \{T\}^{(ne)} dx dy =$$

$$\iint N_i \dot{Q}\, dx\, dy + \oint N_i k \left(\frac{\partial N_j}{\partial x} n_x + \frac{\partial N_j}{\partial y} n_y \right) \{T\}^{(ne)}\, dB =$$

$$= \oint N_i k \frac{\partial T}{\partial n}^{(e)} dB + \iint N_i \dot{Q}\, dx\, dy \qquad (3.6)$$

The second term on the RHS is the heat generation contribution and the first term is from heat transfer boundary conditions.

For evaluating the integral expressions in equation (3.6), *Gauss-Legendre* numerical quadrature is used. The numerical integration can be performed easily by introducing local coordinates (ζ, η) as shown in Fig. (3.1). In terms of these coordinates, any quadrilateral element is mapped onto a square with ζ and η variations over the range, $\pm$ 1. In the present work, 4 - noded quadrilateral elements have been used for which the shape functions are given by

$$N_i = \frac{1}{4}\left(1 + \xi_i \xi\right)\left(1 + \eta_i \eta\right), \tag{3.7}$$

and, i = 1, 2, 3, 4 within each element.

(ii) *SPECIES-DIFFUSION EQUATION*

The diffusion equation is given by :

$$\frac{\partial c}{\partial t} = \frac{\partial}{\partial x}\left(D\frac{\partial c}{\partial x}\right) + \frac{\partial}{\partial y}\left(D\frac{\partial c}{\partial y}\right) - \left(u\frac{\partial c}{\partial x} + v\frac{\partial c}{\partial y}\right) \tag{3.8}$$

In a similar manner as done in the case of energy equation, the residue equation is obtained as :

$$R^{(e)} = \frac{\partial c}{\partial t}^{(e)} - \frac{\partial}{\partial x}\left(D\frac{\partial c}{\partial x}^{(e)}\right) - \frac{\partial}{\partial y}\left(D\frac{\partial c}{\partial y}^{(e)}\right) + \left(u\frac{\partial c}{\partial x}^{(e)} + v\frac{\partial c}{\partial y}^{(e)}\right), \tag{3.9}$$

where,

$$C^{(e)} = \{N(x,y)\}\ \{C(t)\}^{(ne)} \tag{3.10}$$

The weighted residue equations are given by :

$$\iint N_i \left[\frac{\partial c}{\partial t}^{(e)} - \frac{\partial}{\partial x}\left(D\frac{\partial c}{\partial x}^{(e)}\right) - \frac{\partial}{\partial y}\left(D\frac{\partial c}{\partial y}^{(e)}\right) + \left(u\frac{\partial c}{\partial x}^{(e)} + v\frac{\partial c}{\partial y}^{(e)}\right)\right] dxdy = 0 \tag{3.11}$$

Applying Green's theorem, the final form of the residue equations are obtained as :

$$\iint N_i N_j \{\dot{C}\}^{(ne)} dx\, dy + \iint D\left(\frac{\partial N_i}{\partial x} \frac{\partial N_j}{\partial x} + \frac{\partial N_i}{\partial y} \frac{\partial N_j}{\partial y} \right) dx\, dy \; \{C\}^{(ne)} +$$

$$\iint N_i \left(u \frac{\partial N_j}{\partial x} + v \frac{\partial N_j}{\partial y} \right) dx\, dy \{C\}^{(ne)} = \oint N_i \, D\left(\frac{\partial c}{\partial x} n_x + \frac{\partial c}{\partial y} n_y \right) dB =$$

$$\oint N_i D \frac{\partial c}{\partial n} \, dB \qquad (3.12)$$

The transient term (first term on the LHS) in equation (3.12) is handled by finite difference approach. There are essentially three types of discretization schemes for marching in time. These are :

(i) Implicit scheme

(ii) Explicit scheme

(iii) Crank-Nicolson scheme

In the implicit procedure, the time derivative $\dot{C}$ is evaluated at t_{n+1}, while marching from the n^{th} time level (t_n) to the $(n+1)^{th}$ time level (t_{n+1}). For the explicit scheme, $\dot{C}$ is evaluated at t_n , while for the Crank - Nicolson it is evaluated at $t_{n+\frac{1}{2}}$. A generalized implicit / explicit time discretization can be employed by using the expression :

$$\dot{C} = (1 - \theta) \{\dot{C}\}_{t_n} + \theta \{\dot{C}\}_{t_{n+1}} , \qquad (3.13)$$

where $\ominus$ is a fraction between 0 to 1.

The transient discretized species finally obtained as :

$$\left(\frac{1}{\Delta t}\,[MASS] + \ominus\,[STIFFNESS]\right)\{C\}_{n+1}^{(ne)} = \Delta t\,\{F\} + [MASS]\{C\}_{n}^{(ne)}$$

$$- (1-\ominus)\,\Delta t\,[STIFFNESS]\{C\}_{n}^{(ne)}, \qquad (3.14)$$

where,

$$[MASS] = \iint N_i N_j\,dx\,dy$$

$$[STIFFNESS] = \iint D\left(\frac{\partial N_i}{\partial x}\frac{\partial N_j}{\partial x} + \frac{\partial N_i}{\partial y}\frac{\partial N_j}{\partial y}\right) dx\,dy$$

$$+ \iint N_i\left(u\frac{\partial N_j}{\partial x} + v\frac{\partial N_j}{\partial y}\right) dx\,dy$$

$$\text{and,} \qquad \{F\} = \oint N_i D\frac{\partial c}{\partial n}\,dB$$

During computations the implicit scheme has been used and hence $\ominus$ =1. The time step (Δt) has been chosen in the range (5 to 20) seconds.

3.3 BOUNDARY CONDITIONS

Modelling of boundary conditions is as important as the modelling of differential equations themselves. In fact,

experience reveals that the toughest part of problem formulation is the prescription of proper boundary conditions.

Surfaces (1), (4), (5), (9) have convective heat transfer boundary condition, with the overall heat transfer coefficient and ambient temperature given as input data.

The weighted residual form of the convective boundary condition is -

$$\oint N_i k\frac{\partial T}{\partial n}\, dB = - \oint N_i h'\left(T - T_{amb}\right)dB$$

$$= - \oint N_i h' T\, dB \; + \oint N_i h' T_{amb} dB \qquad (3.15)$$

Expanding the temperature as $T = \sum_{i=1}^{4} N_j T_j$, the matrix contributions of convective heat loss boundary conditions are given by :

$$\oint N_i k\frac{\partial T}{\partial n}\, dB = \left[\oint N_i h' N_j dB\right]\,[T_j] - \left[\oint N_i h' T_{amb} dB\right] \qquad (3.16)$$

On the surface(10), heat flux is zero. Hence,

$$-k\frac{\partial T}{\partial n} = 0 \qquad (3.17)$$

The rest of the surfaces are having ambient temperature boundary condition, and these surfaces are handled by supplying

boundary temperature value in the input data.

In case of transient diffusion solution, only surfaces (2), (3), (7), (8) are having prescribed (given value) boundary conditions and other surfaces have zero flux condition.

3.4 ELEMENT ASSEMBLY

In the previous section, the elemental contributions to the left hand side coefficient matrix and right hand side vector have been discussed in detail for the four noded isoparametric quadrilateral elements. These elemental contributions are assembled into a global matrix equation by adding the entries corresponding to each nodal variable from neighbouring elements appropriately.

The boundary integral contributions on both the left and right hand sides of the matrix equation are also incorporated as discussed in the previous section. This assembly procedure results in a matrix equation of the form :

$$[A]\{X\} = \{B\}$$

where,

[A]= coefficient matrix

{X}= solution vector of temperature / concentration

obtain the following quantities :

(i) Isotherm plots

(ii) Graphs for the variation of interfacial temperature

(iii) Iso-concentration plots

(iv) Iso-yield stress plots

(v) Approximate wear profiles

ISOTHERMS : Temperature has been predicted for all the nodes in the domain. Using linear interpolation, it is possible to estimate temperature at any point across the element boundary. The coordinates of points with same temperature are calculated using this procedure and joined using smooth curves. At a glance, isotherms give a clear idea about the temperature distribution in the domain.

ISOCONCENTRATION CURVES : Once the temperature field is available in the vicinity of the cutting tool tip, the nodal values of carbon concentration can be calculated easily using equation (3.9). Iso-concentration curves are then plotted to visually depict the extent of diffusion transport, at different times.

ISO-YIELD STRESS CURVES : Based on the nodal temperature and concentration values, the local yield stress has been calculated as discussd in chapter 2. Then contours of constant yield shear stress in the tool material have been plotted. Comparing this with the actual stress in the tool material, the wear profile can be obtained.

3.7 PROGRAM FOR FINITE ELEMENT ANALYSIS

The programming work is divided into two parts :

(i) Program for grid generation

and, (ii) program for finite element analysis.

In the grid generation program, coordinates of all the points within the solution domain and the elemental connectivity are calculated. These are used in the finite element analysis.

Fig. (3.3) gives the flow chart of the analysis program.

The main program calls the subroutines DINPUT and ITERAT which in turn call the other subroutines.

Subroutine DINPUT reads and returns all the input data such as cutting conditions, initial conditions, boundary conditions, nodal coordinates, elemental connectivity data and prescribed parameters like ambient temperature and material properties at ambient temperature. The whole input data is in dimensional form. Some of the inputs are checked for correction by two routines named DIAGN1 and DIAGN2.

Subroutine ITERAT calls the FRONTS subroutine for solving assembled matrix equation. This subroutine begins the problem with initial values of all the nodal variables. This routine also calls WRITER subroutine to write the nodal values of the variables if the solution has converged.

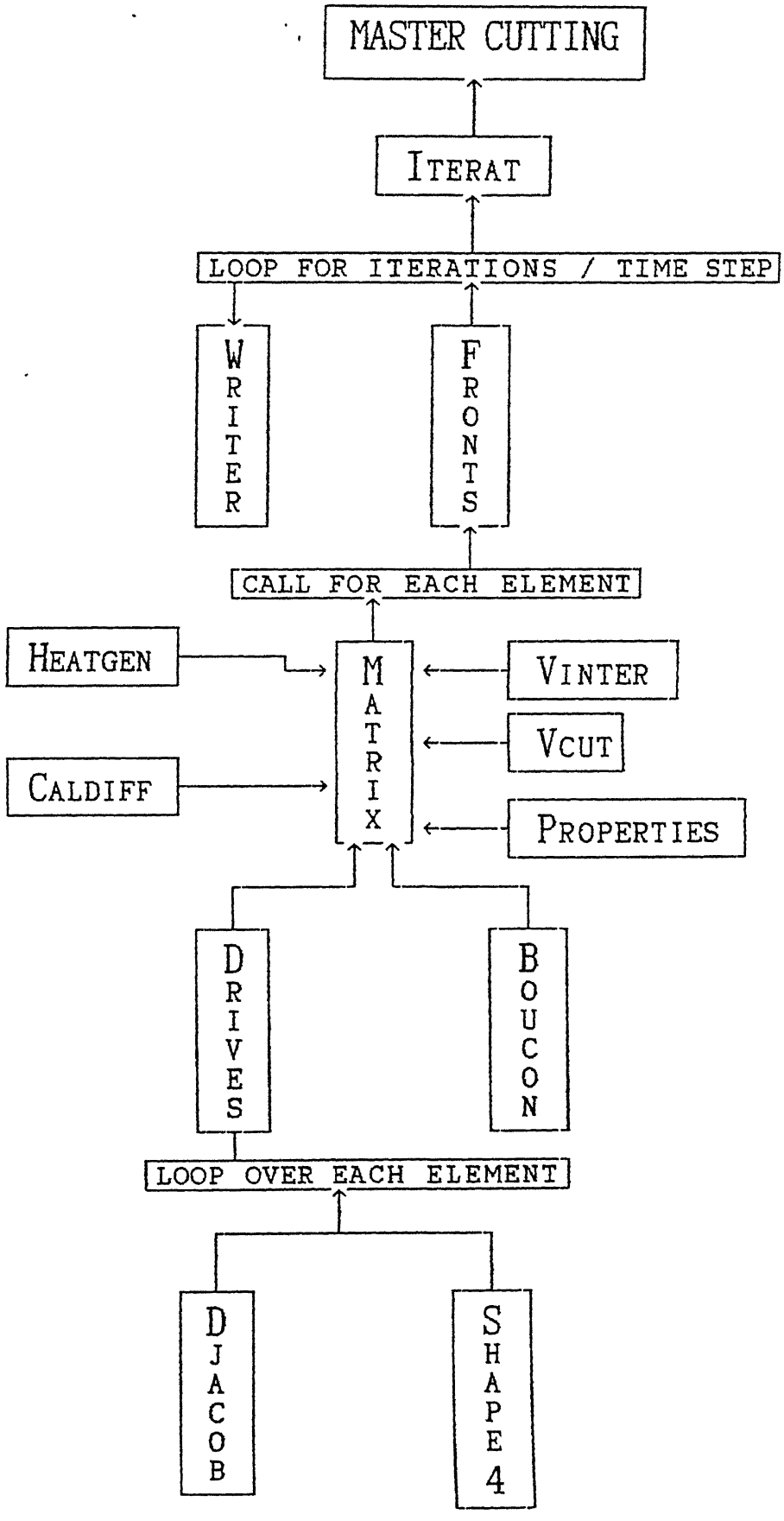

FIG. 3.3 : FLOW CHART OF THE FEM PROGRAM

FRONTS also calls the MATRIX subroutine which calculates the element fluid matrix 'flumx'. This fluid matrix consists of the elemental contributions of the governing equations to form the coefficient matrix. Similarly elemental right hand side vector is also calculated here. Subroutine DRIVES is called within MATRIX, which in turn calls the subroutines SHAPE4 and DJACOB to calculate shape functions and their derivatives. MATRIX subroutine also calls subroutines VINTER, VCUT, HEATGEN and PROPERTIES for calculating quantities such as the inter facial velocity, cutting velocity, heat generation and material properties respectively for the temperature solution. Similarly, during the solution of the species diffusion problem, the MATRIX subroutine calls the subroutines of CALDIFF, VINTER, VCUT and PROPERTIES for calculating the diffusion coefficient, inter-facial velocity, cutting velocity and material properties.

The boundary conditions are implemented in BOUCON which is called in MATRIX before it returns to FRONTS. This is called for only boundary elements.

3.8 CLOSURE

Although the formulation and the programme code developed in the present study are general, they could not be applied to a variety of realistic situations involving the wear of HSS, WC and

coated tools. The main reason for this was the lack of data on material properties, especially on the diffusion coefficients and and regarding the effect of alloying component concentration on the strength of the tool material. Also data on the machining conditions at high cutting speeds were scarce. Therefore, only a few model studies could be conducted and even here, diffusion wear was important only for some cases. With more complete data, the analysis can be applied to several practical situations to study tool wear.

CHAPTER 4

RESULTS AND DISCUSSIONS

Using the Finite Element solution procedure discussed in the previous chapter, temperature and concentration fields have been predicted for a variety of typical machining conditions for HSS and carbide tools. These have been further processed to obtain the variations in the local yield stress value, finally leading to an estimate of the crater wear length in the case of the HSS tools. For carbide tools, the post-processing was not possible on account of data scarcity on variation of tool hardness. The results obtained from the analysis are discussed below.

4.1 TEMPERATURE RESULTS

For HSS tools, results of earlier researchers are available mainly in the low cutting speed conditions. Although the diffusion effect as well as the tool wear will be negligibly small for such conditions, computations have been made for low speed situations also with the intention of comparing the temperature predictions.

In Figs. (4.1-4.4), the steady-state isothermal contours within the tool and the chip have been presented. The predicteed

TOOL MATERIAL = HSS
$\alpha = 41^{\circ}$
V = 24.76 m/min

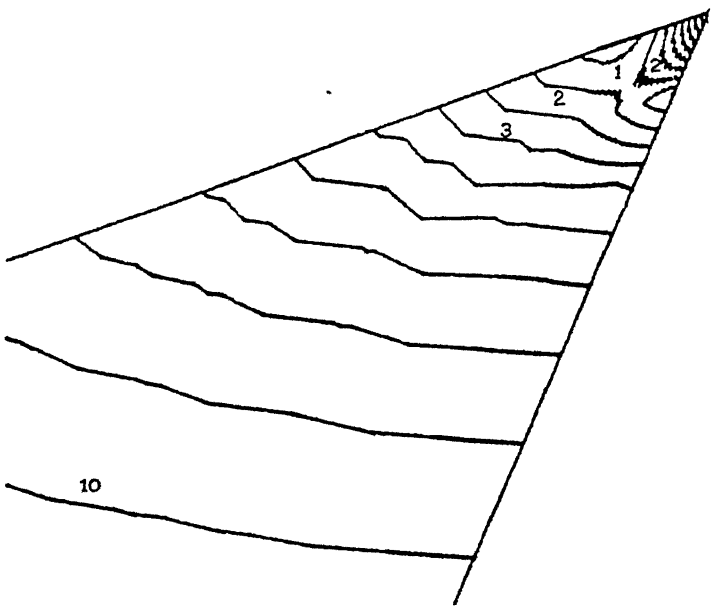

1. T = 826.285 K
2. T = 786.285 K
3. T = 746.285 K
10. T = 466.285 K
ΔT = 40 K
(IN TOOL)

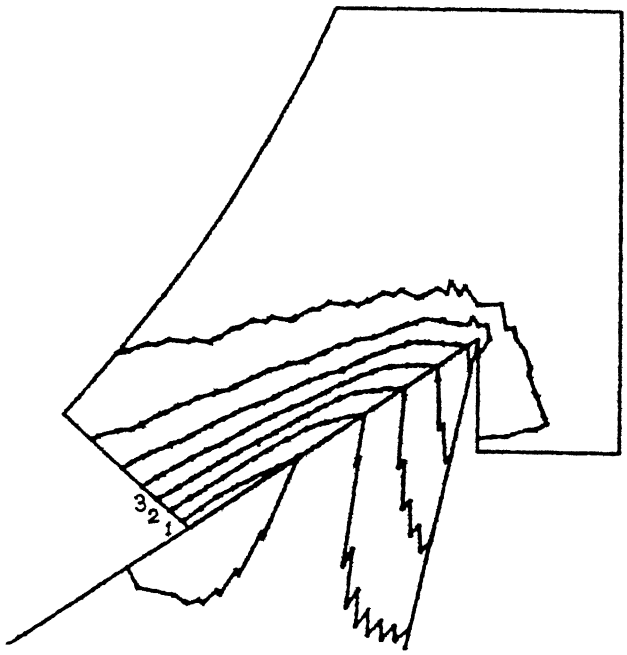

1. T = 826.285 K
2. T = 506.285 K
3. T = 346.285 K
ΔT = 80 K
(IN CHIP)

FIG. 4.1 : TEMPERATURE CONTOURS

TOOL MATERIAL = TUNGSTEN CARBIDE
$\alpha = 20^{\circ}$
V = 130.73 m/min

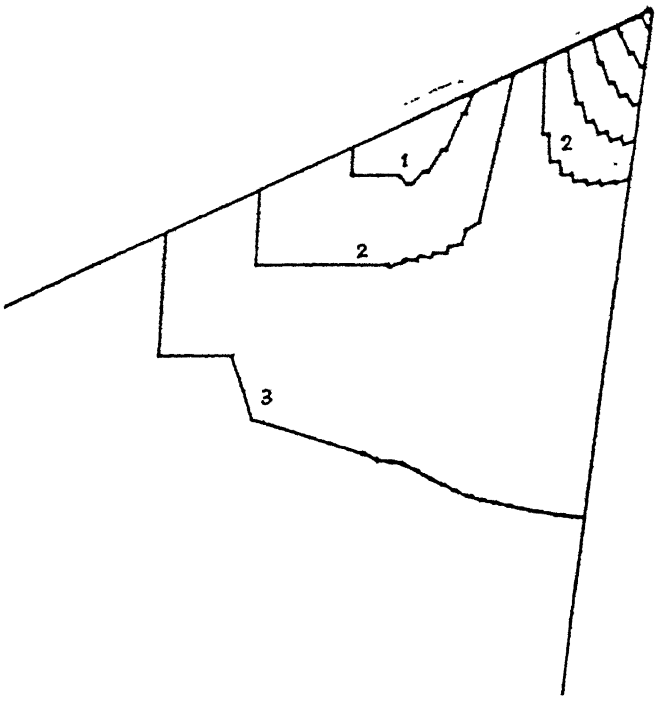

1. T = 1178.28 K
2. T = 1058.28 K
3. T = 938.28 K
ΔT = 120 K
(IN TOOL)

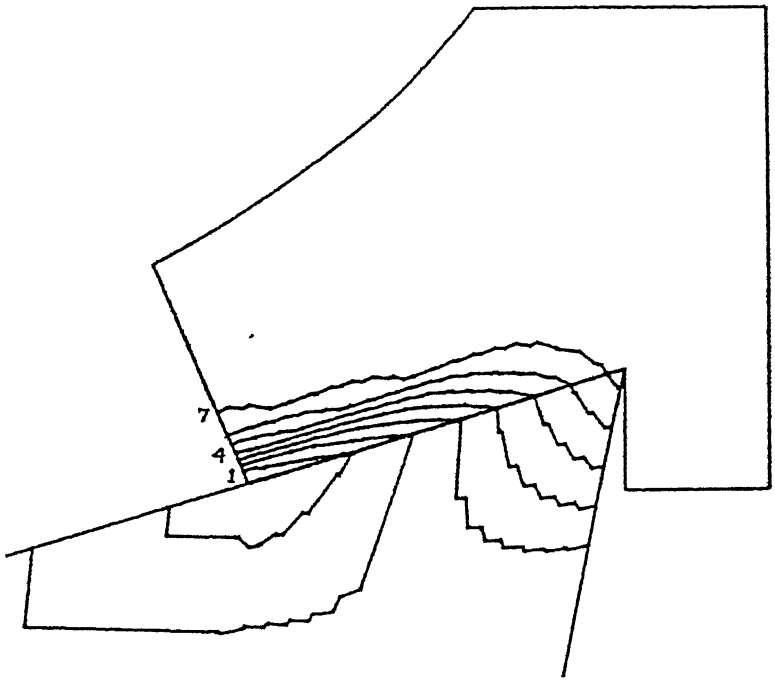

1. T = 1178.28 K
4. T = 818.28 K
7. T = 458.28 K
ΔT = 120 K
(IN CHIP)

FIG. 4.2 : TEMPERATURE CONTOURS

TOOL MATERIAL = HSS
$\alpha = 25^{\circ}$
V = 140 m/min

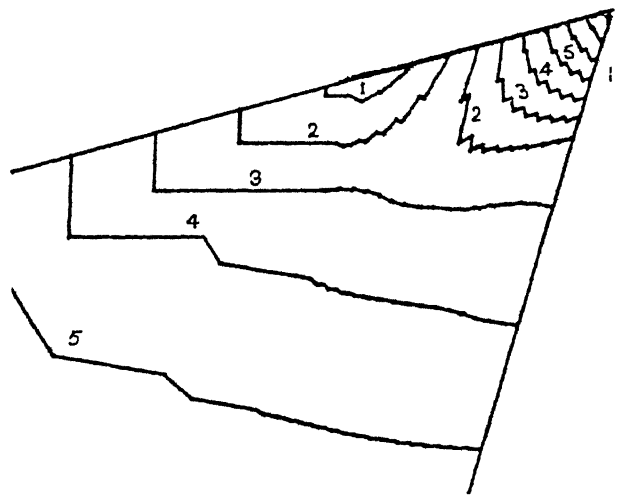

1. T = 1600 K
2. T = 1460 K
3. T = 1320 K
4. T = 1180 K
5. T = 1040 K

(TOOL)

FIG. 4.3 : TEMPERATURE CONTOURS

TOOL MATERIAL = HSS
$\alpha = 20^{\circ}$
V = 154.6 m/min

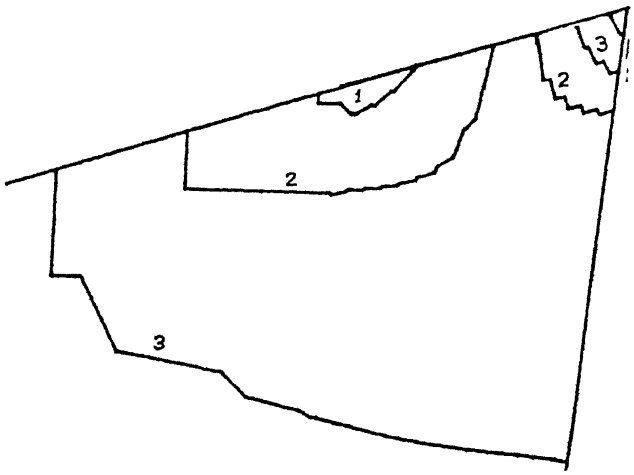

(TOOL)

1. T = 1037.18 K
2. T = 897.18 K
3. T = 757.18 K
ΔT = 140 K

FIG. 4.4 : TEMPERATURE CONTOURS

contours are in reasonable agreement with the results of *Murarka et al.* [1979] and *Tay et al.* [1974]. The maximum temperature isotherm occurs slightly away from the cutting edge on the chip-tool interface. This is obviously the result of metal getting heated up through primary and secondary deformation zones sequentially. In the chip also, high temperature zone occurs adjacent to the interface as expected. It is clear that the maximum temperature increases with cutting speed, due to the larger rate of heat production (caused by the plastic deformation).

The variation of interfacial temperature with distance from the cutting edge are shown in Figs. (4.5) and (4.6), for two different cutting conditions. The predictions of the present analysis have been compared with those of *Murarka et al.* [1979]. Although there is reasonable agreement in the predicted trends, some differences are also observed. In the present analysis, the variations in material thermal properties such as the thermal conductivity and specific heat have been fully taken into account. Also a variable shear stress has been assumed to exist on the chip-tool interface as known from independent stress measurements. *Murarka* and co-workers assumed constant properties and uniform interfacial shear stress. Their predictions were justified on the basis of comparing the theoretical results for the average tool tip temperature with actual measurements by tool thermocouple method. The average tool tip temperature predicted from the

TOOL MATERIAL = HSS
– – – MURARKA et al.
——— PRESENT MODEL

$\alpha = 20^{\circ}$
V = 24.68 m/min

T_{av}(MURARKA) = 736.87 K
T_{av}(PRESENT MODEL) = 723.96 K

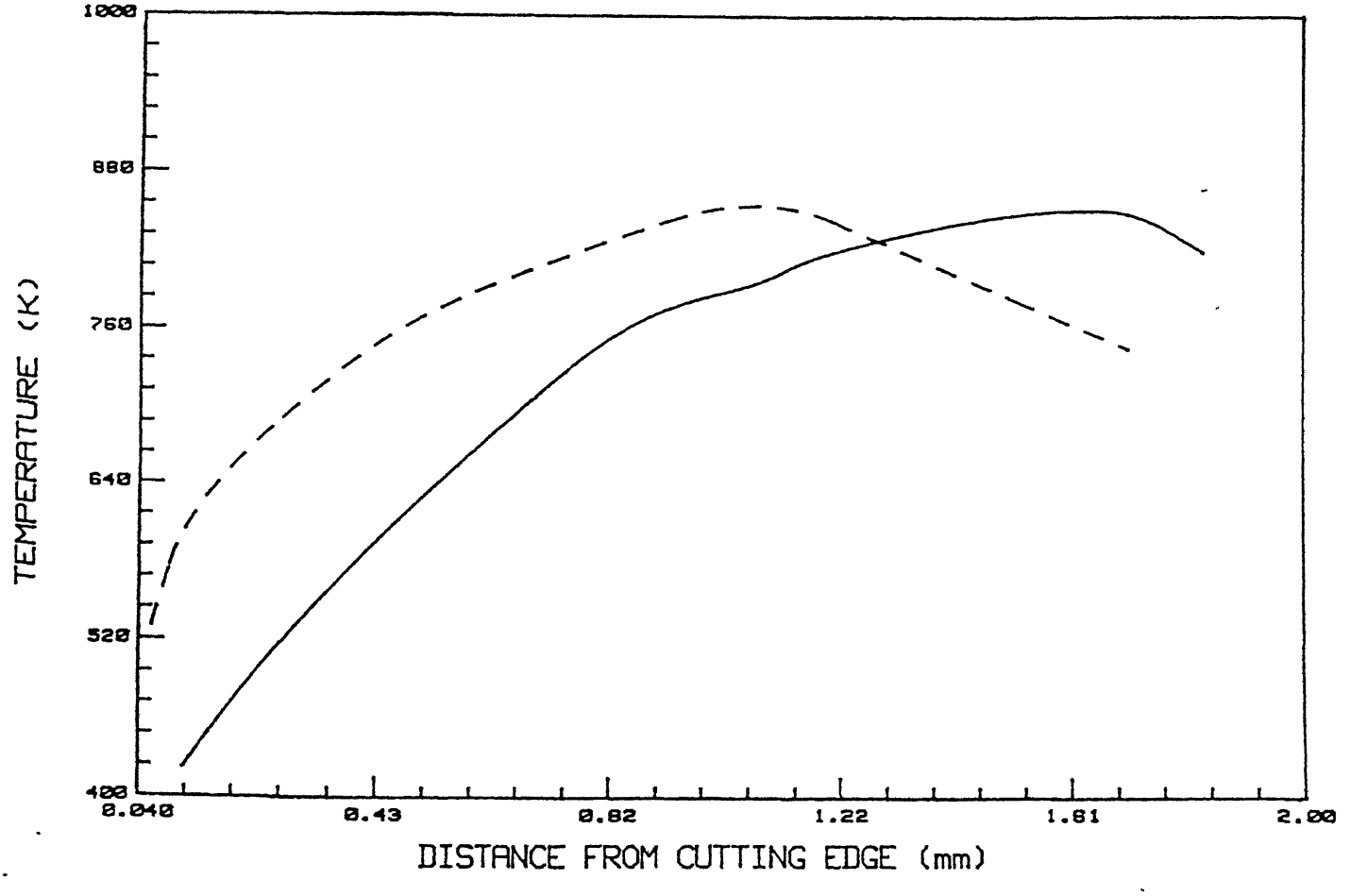

FIG. 4.5 : VARIATION OF INTERFACIAL TEMPERATURE

TOOL MATERIAL = HSS
- - - MURARKA et al.
——— PRESENT MODEL

$\alpha = 41^{\circ}$
V = 24.76 m/min

T_{av} (MURARKA) = 718.76 K
T_{av} (PRESENT MODEL) = 730.45 K

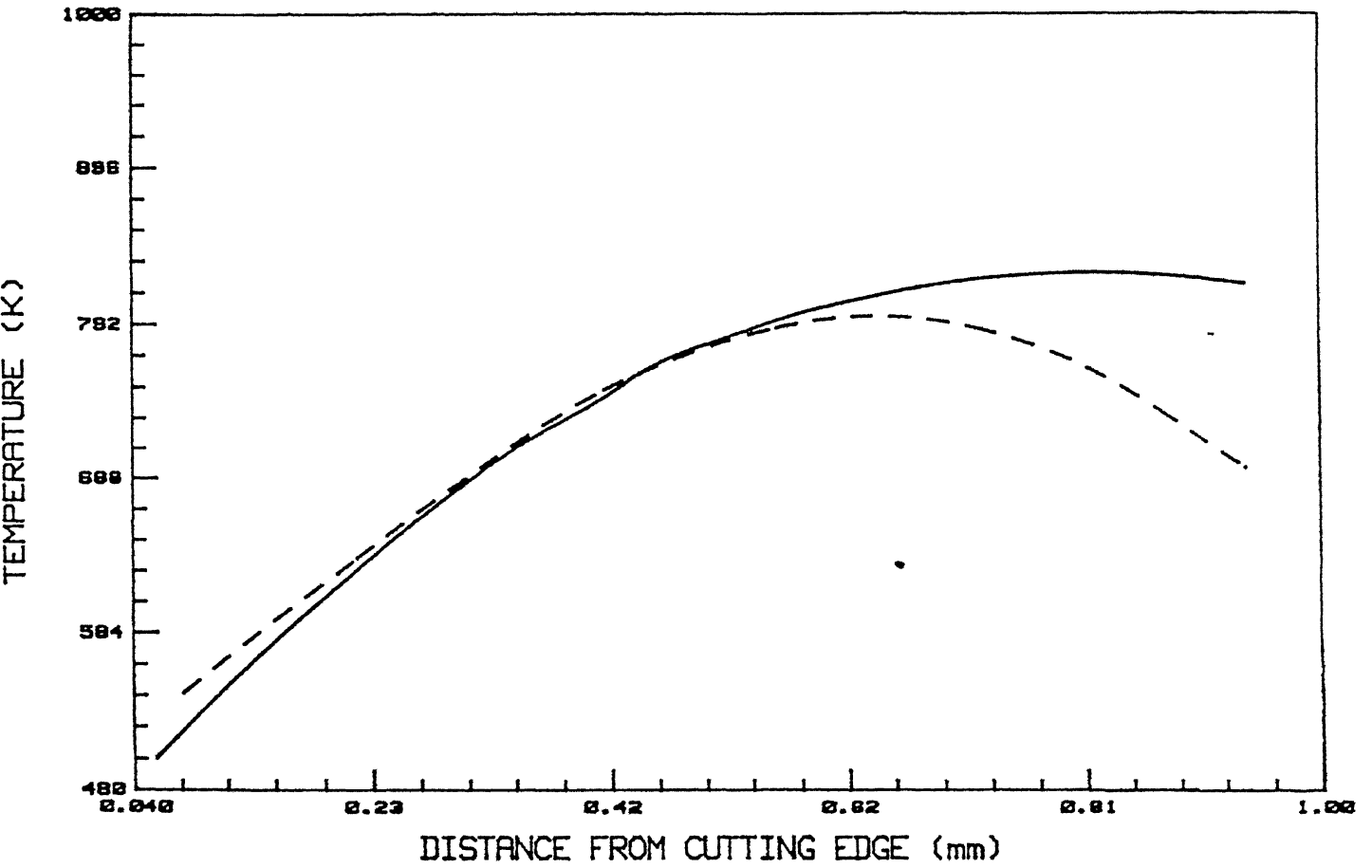

FIG. 4.6 : VARIATION OF INTERFACIAL TEMPERATURE

present analysis is quite close to that obtained by *Murarka et al.* [1979].

4.2 CONCENTRATION PROFILES

In Fig. (4.7), the concentration profiles at the various times are presented for the carbide tool. It is evident from these figures that diffusion of carbon within the tool gets depleted in course of time in the region close to the interface. The depth affected by carbon diffusion increases with time in the beginning, but eventually a steady-state is approached. The reason for this lies in the fact that the high temperature zone occurs close to the chip-tool interface. Diffusion being a process which is very sensitive to the temperatutre (exponential dependence), a region close to the interface is affected. The concentration profiles obtained for the HSS tool (Fig. (4.8)) are similar to those for the carbide tool.

A point to be noted regarding the results of Figs. (4.7-4.8) is that these correspond to fairly high cutting speeds. At low speeds, the temperature level is also low and diffusion is virtually non-existent.

4.3 YIELD STRESS CONTOURS

In Figs. (4.9 and 4.10), the constant yield stress contours

TOOL MATERIAL = TUNGSTEN CARBIDE
$\alpha = 20^{\circ}$
V = 130.76 m/min

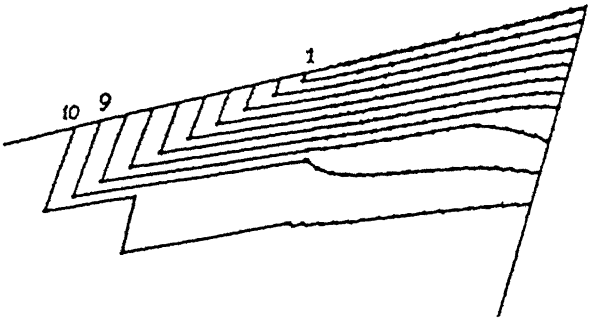

1. c = 0.557 %
9. c = 0.621 %
10.c = 0.629 %
Δc = 0.008 %
AFTER 5 SECONDS

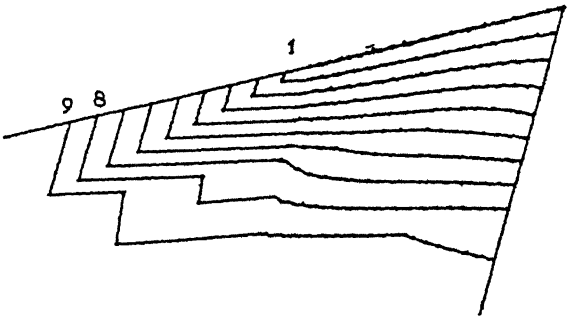

1. c = 0.295 %
8. c = 0.645 %
9. c = 0.695 %
Δc = 0.05 %
AFTER 15 SECONDS

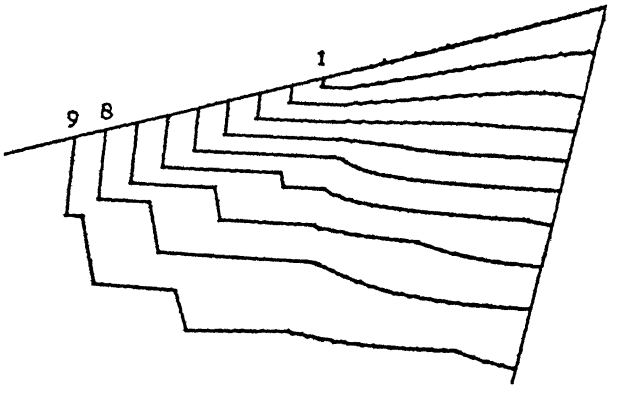

1. c = 0.174 %
8. c = 0.734 %
9. c = 0.814 %
Δc = 0.08 %
AFTER 25 SECONDS

FIG. 4.7 : CONTOURS OF CARBON CONCENTRATION IN TOOL

TOOL MATERIAL = HSS
$\alpha = 20^{\circ}$
V = 154.6 m/min
TIME = 10 min

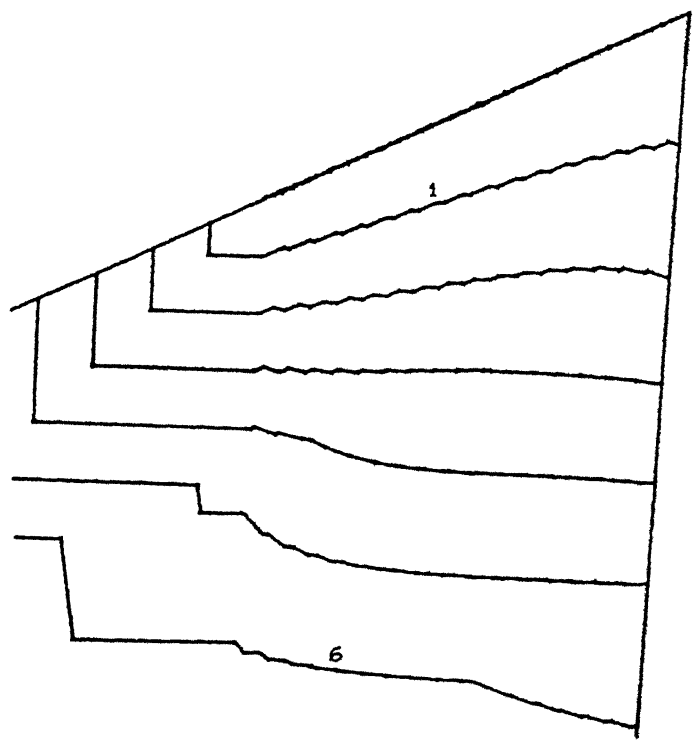

1. c = 0.217 %
6. c = 0.717 %
Δc = 0.1 %

FIG. 4.8 : CONTOURS OF CARBON CONCENTRATION IN TOOL

TOOL MATERIAL = HSS
$\alpha = 22^{\circ}$
V = 150 m/min
TIME = 10 min

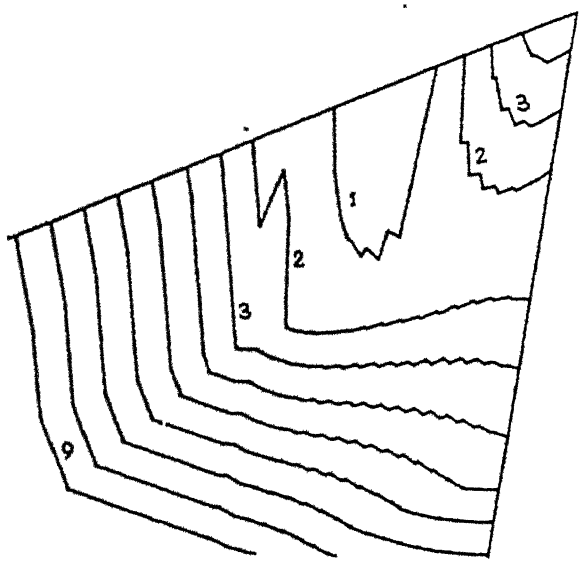

1. σ_{YS}= 501.714 N/mm^2
2. σ_{YS}= 541.714 N/mm^2
3. σ_{YS}= 581.714 N/mm^2
9. σ_{YS}= 821.714 N/mm^2

$\Delta\sigma_{YS}$= 40 N/mm^2

FIG. 4.9 : YIELD STRESS VARIATION IN TOOL

TOOL MATERIAL = HSS
$\alpha = 20^{\circ}$
V = 154.6 m/min
TIME = 10 min

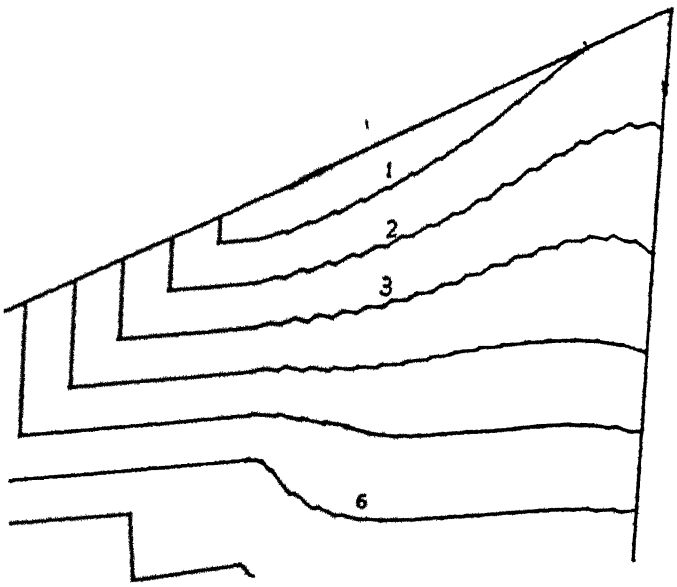

1. σ_{YS} = 501.69 N/mm^2
2. σ_{YS} = 601.69 N/mm^2
3. σ_{YS} = 701.69 N/mm^2
6. σ_{YS} = 1001.69 N/mm^2

$\Delta\sigma_{YS}$ = 100 N/mm^2

FIG. 4.10 : YIELD STRESS VARIATION IN TOOL

within the tool have been plotted. The material strength decreases considerably (almost by a factor of 5-6) near the chip-tool interface due to both high temperature conditions and the depletion of the alloying element (carbon). The contours have shapes approximately similar to that of the crater. If a detailed stress analysis is done for the tool side, the yield stress contours will be useful for applying local yield criterion to predict the depth of crater wear. It must, however be cautioned that wear being a dynamic phenomenon, a dynamic stress analysis is necessary.

4.4 CRATER LENGTH PREDICTIONS

In Figs. (4.11-4.15), the yield stress values along the interface are compared against the assumed actual stress variation. Since it is reasonable to expect that wear should occur if yield stress is less than the actual stress, the zone where this inequality holds should be prone to wear. Thus, the approximate length of the crater can be predicted for a given machining time by comparing the local yield stress and actual stress value.

In the present work, due to time limitations, it was not possible to perform a complete stress analysis of the tool portion. Coupling the stress predictions with transient thermal and diffusion analysis within the tool, the extent of diffusion

TOOL MATERIAL = HSS
TIME = 10 min
- - - YIELD STRESS
——— ACTUAL STRESS

$\alpha = 20^{\circ}$
V = 120 m/min
T_{max} = 1634.1 K
fh = 3587.7 N
fv = 1190.7 N

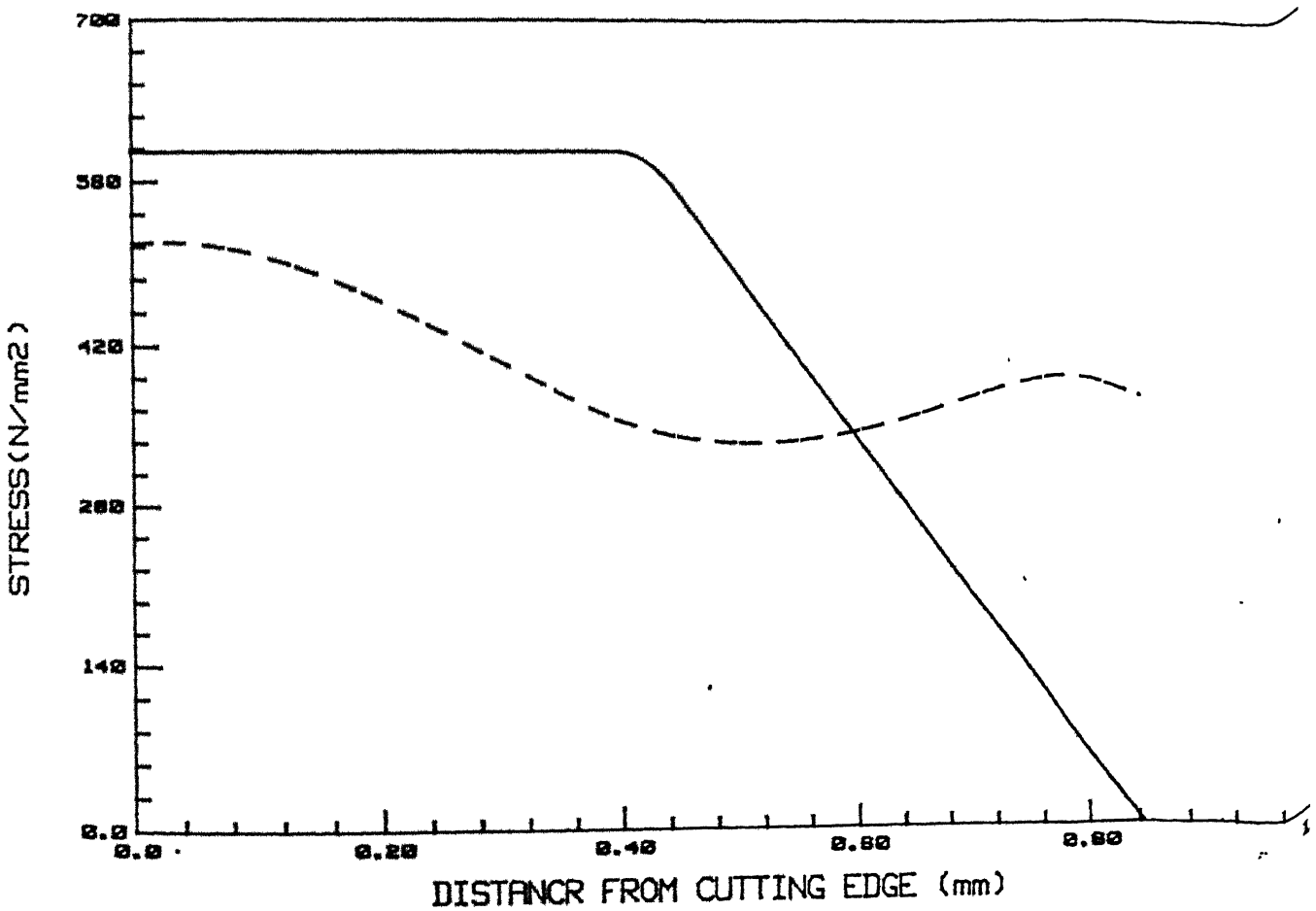

FIG. 4.11 : COMPARISON OF INTERFACIAL STRESSES AND ESTIMATION OF CRATER LENGTH

TOOL MATERIAL = HSS
TIME = 10 min
— YIELD STRESS
----- ACTUAL STRESS

$\alpha = 25^{\circ}$
V = 140 m/min
T_{max} = 1622.81 K
fh = 3610.2 N
fv = 1210.8 N

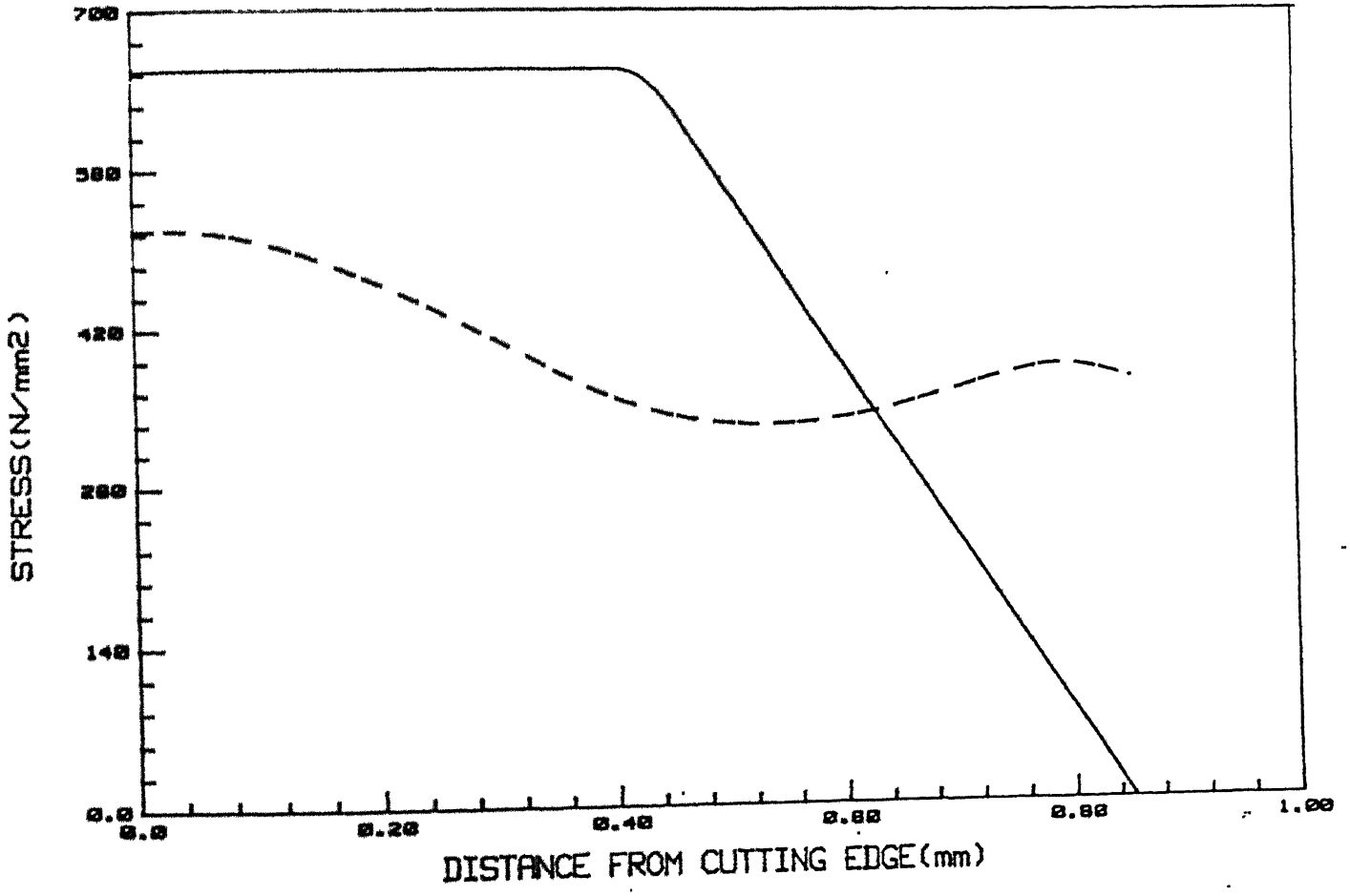

FIG. 4.12 : COMPARISON OF INTERFACIAL STRESSES AND ESTIMATION OF CRATER LENGTH

TOOL MATERIAL = HSS
TIME = 10 min
- · YIELD STRESS
-- - ACTUAL STRESS

$\alpha = 22^{\circ}$
V = 150 m/min
T_{max} = 1628.96 K
fh = 3604.6 N
fv = 1200.3 N

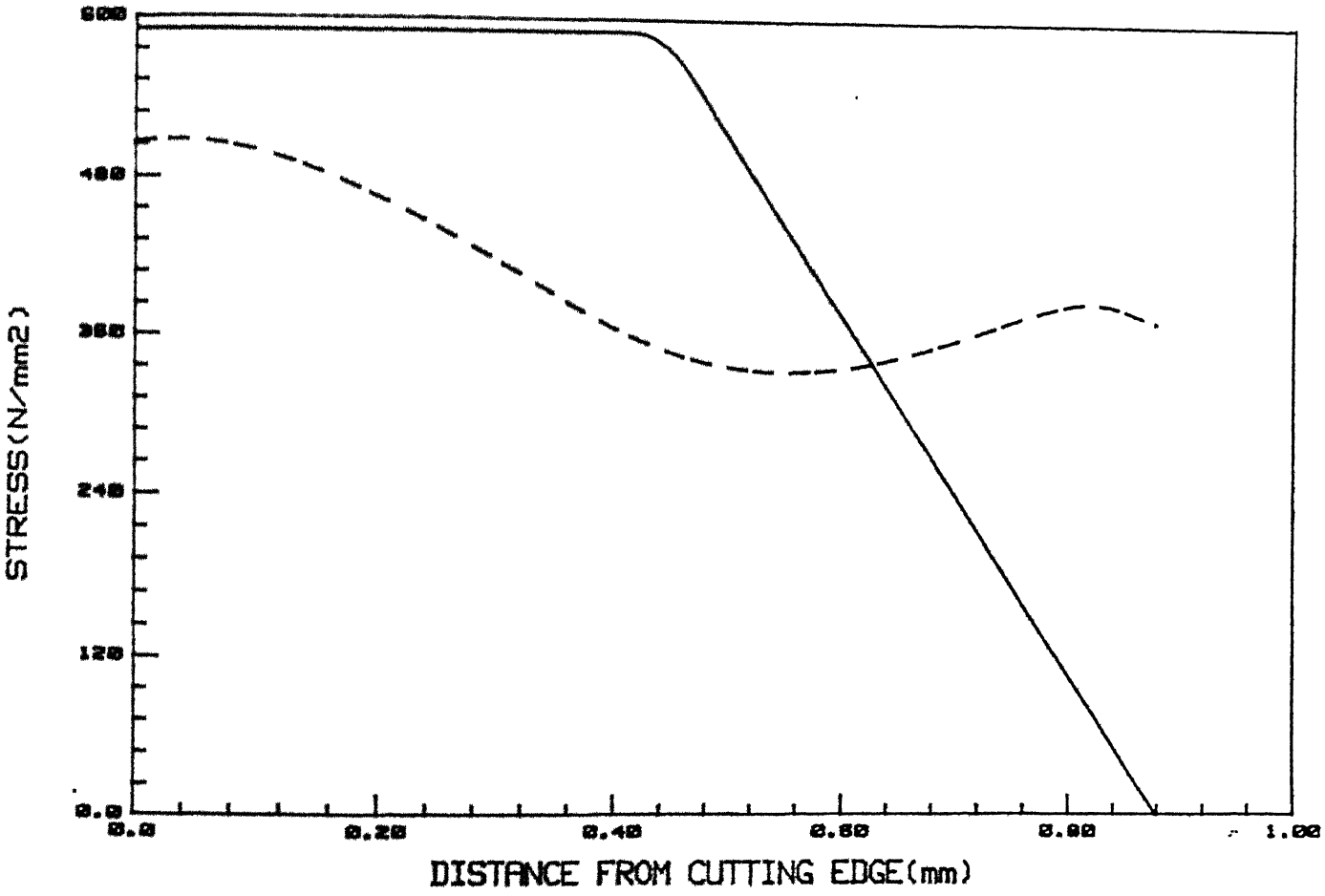

FIG. 4.13 : COMPARISON OF INTERFACIAL STRESSES AND ESTIMATION OF CRATER LENGTH

TOOL MATERIAL = HSS
TIME = 10 min
– – – YIELD STRESS
— — — ACTUAL STRESS

$\alpha = 20^{\circ}$
V = 154.6 m/min
T_{max} = 1037.18 K
fh = 3500.0 N
fv = 1560.0 N

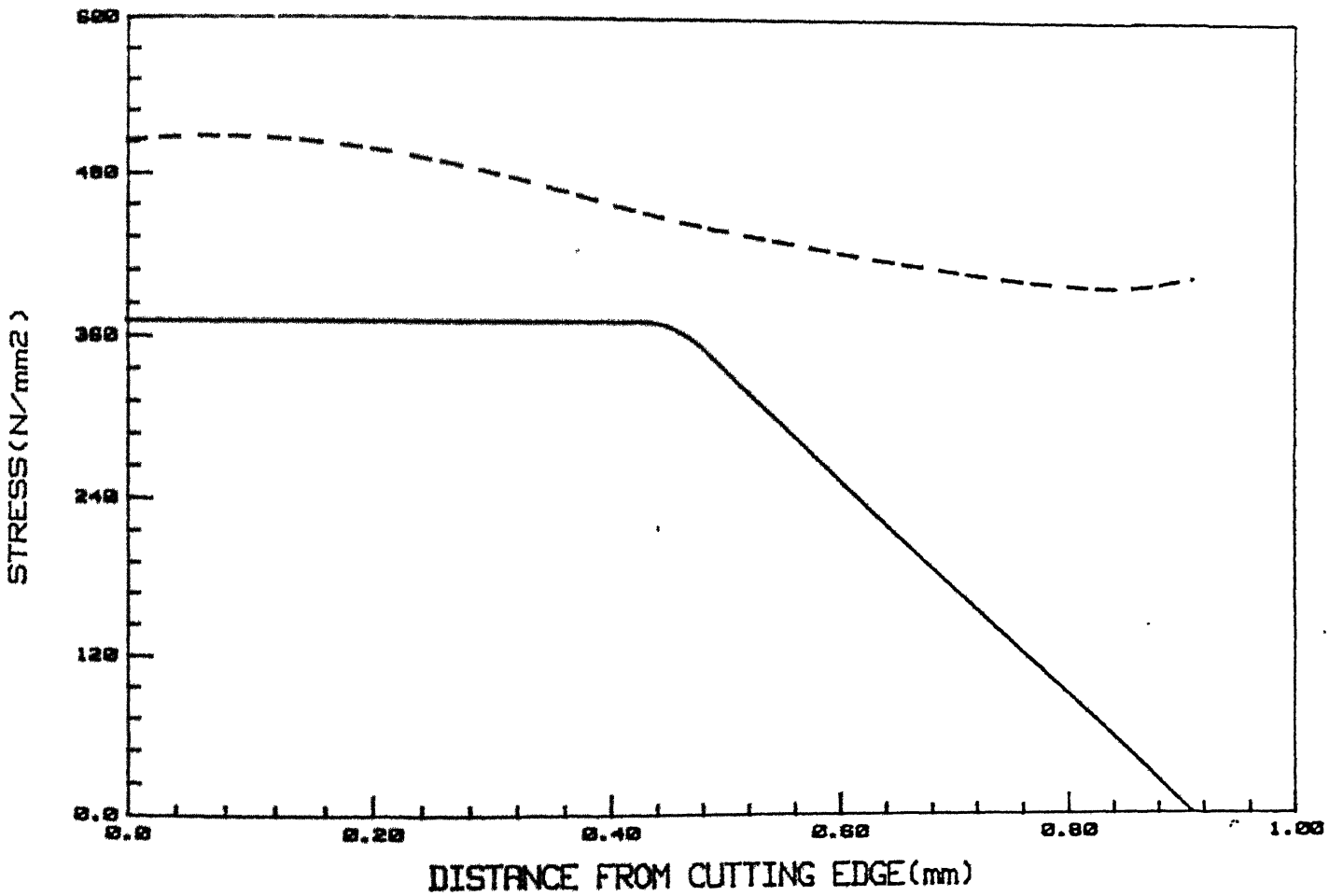

FIG. 4.14 : COMPARISON OF INTERFACIAL STRESSES AND ESTIMATION OF CRATER LENGTH

TOOL MATERIAL = HSS
TIME = 10 mn
- - - YIELD STRESS
——— ACTUAL STRESS

$\alpha = 20^{\circ}$
V = 160 m/min
T_{max} = 1691.67 K
fh = 3520 N
fv = 1260 N

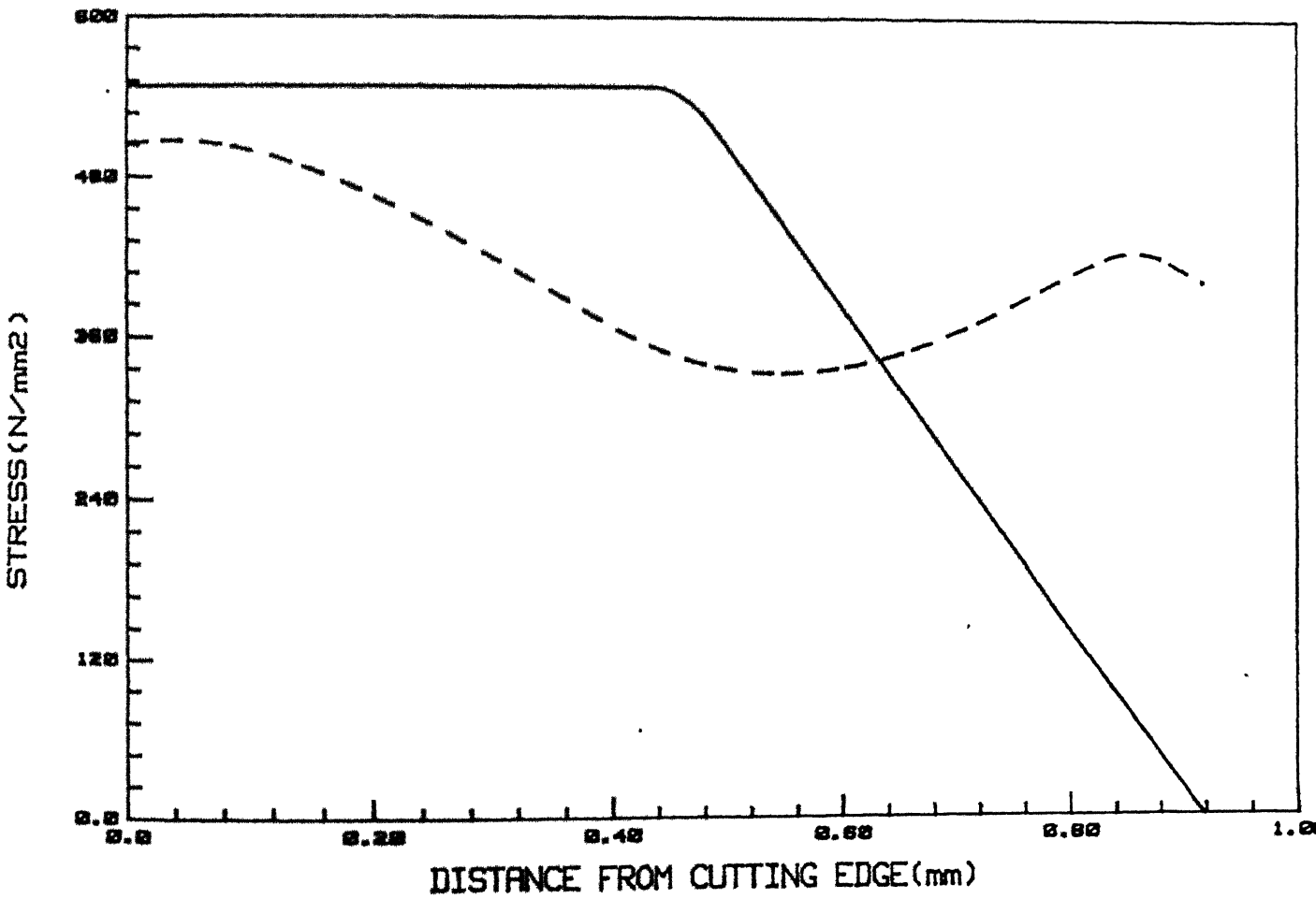

FIG. 4.15 : COMPARISON OF INTERFACIAL STRESSES AND ESTIMATION OF CRATER LENGTH

wear at any instant can be judged. The results of the present study indicate that diffusion wear is important only at elevated temperature conditions (above 900° C). This observation is in agreement with the trends known from practical measurements.

4.5 CONCLUSION

A Theoretical model for estimating the diffusion wear has been proposed, based on the temperature and concentration fields within the tool region. The model proposed here considers carbon diffusion only. However, diffusion of other species can also be incorporated in a similar way and the effect of such diffusion phenomena on tool strength can be analysed. Finally, based on a detailed stress analysis, it is possible to obtain wear profiles at different times.

CHAPTER 5

SUGGESTIONS FOR FUTURE WORK

In the present work, only the heat exchange and diffusion equations have been solved for the sake of simplicity. These can be coupled with a visco-plastic model for the chip region and an elasto-plastic stress analysis of the tool region.

Diffusion of other species such as tungsten, cobalt, chromium, vanadium, molebdenum etc. can be considered. The effects of such difussing species on the tool strength can be studied.

Considering a blunt tool, flank wear can be studied in a similar manner.

Different cutting tool materials (various HSS grades, carbide tools, coated carbide tools etc.) can be studied.

REFERENCES

ON MECHANICS OF CHIP FORMATION

Drucker, D. C., 1949, "*An Analysis of the Mechanics of Metal Cutting*", J. of Appl. Phy., Vol. 20, p. 1013.

Kececioglu, D., 1958, "*Shear Strain-rate in Metal Cutting and its Effects on Shear Flow Stress*", Trans. of ASME, Engrs., Vol. 80, p. 158.

Merchant, M. E., 1944, "*Basic Mechanics of Metal Cutting Process*", J. of Appl. Phy., p. 168. Merchant, M. E., 1945, "*Mechanics of Metal Cutting Process -I*", J. of Appl. Phy., Vol. 16, p. 267.

Merchant, M. E., 1945, "*Mechanics of Metal Cutting Process -II*", Vol. 16, p. 318.

Okushima, K. and Hitomi, K., 1957, "*On Cutting Mechanism of Soft Metals*", Trans. of JSME, Vol. 23, No. 134, p. 674.

Palmer, W. B. and Oxley, P. L. B., 1954, "*The Mechanics of Orthogonal Machining*", Proc. Instn. of Mech. Engrs., Vol. 173, p. 24.

Piispanen, V., 1948, "*Theory of Formation of Metal Chips*", J.of Appl. Phy., Vol. 19, p. 876.

Stevenson, M. G. and Oxley, P. L. B., 1969-70, "*An Experimental Investigation on the Influence of Speed and Scale on the Strain-rate in a Zone of Intense Plastic Deformation*" Proc. of Instn. of Mech. Engrs., Vol. 184, Pt. 1, No. 31, p. 561.

Taylor, F. W., 1907, "*On the Art of Cutting Metals*" Trans. of ASME, Vol. 28, p. 31.

ON PREDICTION OF TEMPERATURE

Blok, H., 1938, Proc. of Instn. of Mech. Engrs., Vol. 152, p. 222.

Dutt, R. P. and Brewer, R. C., 1964, Instt. J. of Production Research., Vol. 4, p. 91.

Hann, R. S., 1951, ASME, p. 661.

Loewen, E. G., and Shaw, M. C., 1954, Trans. of ASME, Vol. 76, p. 217.

Rapier, A. C., 1954, British J. of Appl. Phy., Vol. 5, p. 400.

Trigger, K. J. and Chao, B. T., 1951, Trans. of ASME, Vol. 73, p. 57.

Trigger, K. J. and Chao, B. T., 1954, Trans. of ASME, Vol. 77, p. 1074.

Weiner, J. H., 1955, "*Shear Plane Temperature Distribution in Orthogonal Cutting*", Vol. 77, p. 1331.

ON VISCO-PLASTIC MODELS USING FEM

Balaji, H.S., Muju, M.K. Sundararajan, T., 1986, "*FEM Simulation of the Temperature Distribution in Machining With Coated Carbide Tools*", 12th AIMTDR, IIT Delhi, p. 2044.

Deshpande, A. S., 1992, "*A Study of Metal Cutting by Visco-Plastic Finite Element Formulation and Comparison with Experiments*", M.Tech. Dissertation, Dept. of Mech. Engg. IIT Kanpur.

Komvopoulos, K. and Erpenbeck, S. A., 1991, "*Finite Element Modelling of Orthogonal Metal Cutting*", Trans. of ASME, J. of Engg. for Industry, Vol. 113, p. 253.

Murarka, P. D., Borrow, G. and Hinduja, S., 1979, "*Influence of the Process Variables on the temperature Distribution in Orthogonal Machining Using Finite Element Method*", Int. J. of Mech. Sci., Vol. 21, p. 445.

Sarma, M. C., 1990, "*A Finite Element analysis of Thermal and Deformation Process in Metal Cutting*", M.Tech. Dissertation, Dept. of Mech Engg., IIT Kanpur.

Stevenson, M. G., Wright, P. K. and Chow, J. S., 1983, "*Further Developements in Applying the Finite Element Method to the Calculation of Temperature Distributions in Machining and Comparison with Experiments*", Trans. of ASME, J. of Engg. for Industry., Vol. 105, p. 149.

Strenkowski, J. S. and Carroll, III, J. T., 1985, "*A Finite Element Method of Orthogonal Metal Cutting*", Trans. of ASME, J. of Engg. for Industry. Vol. 107, p. 349.

Strenkowski, J. S. and Moon, Kyoung-Jin., "*Finite Element Prediction of Chip Geometry and Tool/Workpiece Temperature Distribution in Orthogonal Metal Cutting*", 1990, Trans. of ASME, J. of Engg. for Industry, Vol. 112, p. 313.

Tay, A.O., Stevenson, M.G. and de Vahl Davis, G., 1974, "*Using the Finite Element Method to Determine Temperature Distributions in Orthogonal Machining*", Proc. of Inst. of Mech. Engrs., Vol. 188, p. 627.

Tay, A.O., Stevenson, M. G., de Vahl Davis, G. and Oxley, P.L.B., 1976, "*A Numerical Method for Calculating Temperature Distribution in Machining From Force and Shear Angle Measurements*", Int. J. of MTDR, Vol. 16, p. 335.

Zienkiewicz, O.C., Jain, P.C. and Onate, E., 1978, "*Flow of Solids During Forming and Extrusion*", Int. J. of Solids Struct., Vol. 14, p. 15.

Zienkiewicz, O.C., Onate, E. and Heinrichs, 1981, "*A General Formulation of Coupled Thermal Flow of Metals Using Finite Element*", Int. J. of Num. Methods in Engg., Vol. 17, p. 1497.

ON CUTTING TOOL WEAR

Cook, N.H. and Nayak, P. N., 1966, "*The Thermal Mechanics of Tool Wear*", Trans. of ASME, J. of Engg. For Industry, p. 93.

Dawihl, W., 1941, "*Study of Wear of Cemented Carbides*", Stahl und Eisen,Translated by Bruchter, H., Altadena, Calif., Vol. 61, p. 210.

Kannatey-Asibu, E., 1985, "*A Transport Diffusion Equation in Metal Cutting and its Application to Analysis of the Rate of Flank Wear*", Trans. of ASME, Vol. 107, p. 820.

Rubenstein, C., 1975, "*An Analysis of Tool Life Based on Flank Face Wear, Part-I*", Trans. of ASME, 75-WA/Prod-28, p. 1.

Trent, E. M., 1952, "*Some Factor Affecting Wear on Cemented Carbide Tools*", Proc. of Instn. of Mech. Engrs., Vol. 166, p. 64.

Trigger, K. J. and Chao, B. T., 1956, "*The Mechanism of Crater Wear of Cemented Carbide Tools*", Trans. of ASME, p. 1119.

ON METAL MACHINING

Armarego, E. J. A. and Brown, R. H., 1969, "*The Machining of*

Metals", Prentice-Hall, Inc., USA.

Jain, V. K. and Gupta, B. K., 1987, "*Effects of Accelerated Tests on Shear Flow Stress in Machining*", Trans. of ASME, J. of Engg. for Industry, Vol. 109, p. 206.

Sen, G.C. and Bhattacharyya, A., "*Principles of Machine Tools*", Vol. 1, Central Book Agency, Calcutta, India.

Venkatesh, Y. C. and Chandrasekaran, H., 1987, "*Experimental Techniques in Metal Cutting*", Prentice-Hall of India. Pvt. Ltd., New-Delhi.

ON FINITE ELEMENT METHOD

Reddy, J. N., 1986, "*An Introduction to the Finite Element Method*", McGraw-Hill Book Company, Singapore.

Taylor, C. and Huges, T. G., 1981, "*Finite Element Programming of Navier Stokes Equations*", 1st Edn., Pineridge Press Ltd., U.K.

ON PHYSICAL DATA

Americann Soceity for Metals, 1978, "*Metals Hand Book*", 9th Edn.,Vol. 1.

Clark, D.S. and Varney, W.R., 1987, "*Physical Metallurgy for Engineers*", 2nd Edn., CBS Publishers and Distributers, New Delhi.

Hoyle, G., 1988, "*High Speed Steels*", Butterworths, England.
Iron and Steel Institute, 1970, "*Materials for Metal Cutting*".

Kothandaraman, C. P. and Subramanyan, S., 1977, "*Heat and Mass Transfer Data Book*", 3rd Edn., Willey Eastern Ltd., India.

Pollack, H. W., 1988, "*Materials Science and Metallurgy*", 4th Edn., Prentice-Hall.

Raghavan, V., 1984, "*Materials Science and Engineering - A First Course*", 2nd Edn., Prentice Hall of India Pvt. Ltd., New Delhi.

Roberts, G. and Cary, R., 1980, "*Tool Steels*", 4th Edn.

Wells, M. G. H. and Lherbier, L. W., 1980, "*Processing and Properties of High Speed Steels*", A Publication of the Metallurgical Scociety of AIME.

Woldman, N. E., 1959, "*Engineering Alloys*".